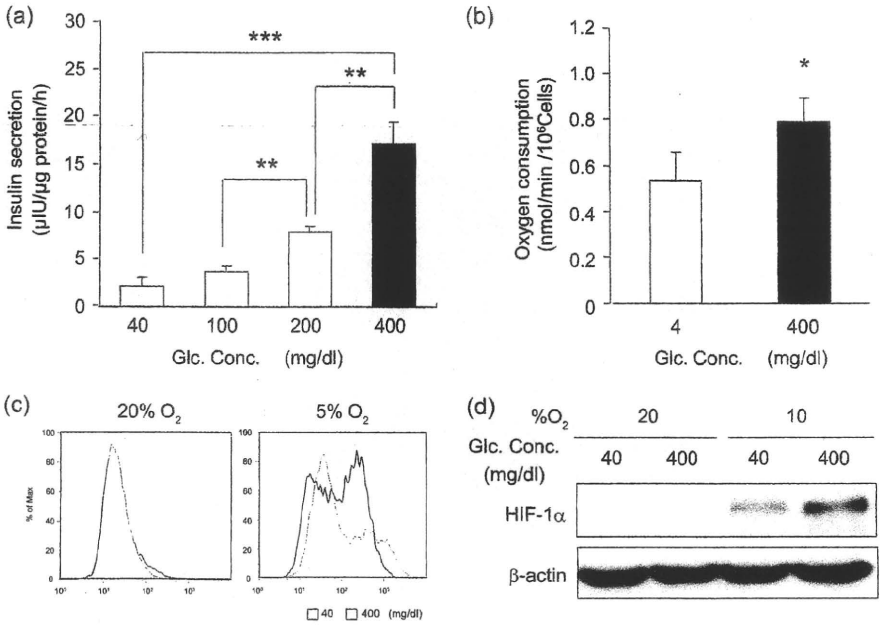

FIGURE 4. **Cellular hypoxia of MIN6 cells was dependent on glucose concentration *in vitro*.** *a*, glucose-dependent insulin secretion. MIN6 cells were stimulated by incubation in various glucose concentrations as indicated for 1 h, and insulin secretion was calculated as the difference between the insulin concentrations of the medium before and after stimulation. *b*, glucose-dependent oxygen consumption. MIN6 cells were cultured with 4 mg/dl for 30 min, and oxygen consumption was measured. Then, 30 min after adding glucose to 400 mg/dl, oxygen consumption was measured. In *a* and *b*, the means ± S.D. (*error bars*) of values from each group are shown (*, $p < 0.05$; **, $p < 0.01$; ***, $p < 0.001$). The experiments were repeated at least three times. *c*, glucose-dependent pimonidazole adduct formation *in vitro*. Shown is flow cytometric analysis of pimonidazole-stained MIN6 cells incubated in 40 or 400 mg/dl glucose as indicated at 20 or 5% oxygen tension for 3 h. *d*, glucose-dependent expression levels of HIF-1α protein. Western blotting of HIF-1α in MIN6 cells cultured under the indicated conditions for 6 h is shown.

BNIP3 (BCL2/adenovirus E1B 19-kDa interacting protein 3), *PGK1* (phosphoglycerate kinase 1), *PDK1* (pyruvate dehydrogenase kinase isozyme 1), and *LDH-A* (lactate dehydrogenase A), that occurred even at 7% oxygen tension, indicate that HIF-1α was transcriptionally active under conditions of mild hypoxia (supplemental Fig. 1*a*). HIF-1α is known to be stabilized by factors other than hypoxia, such as the presence of reactive oxygen species (26, 27). To assess the role of reactive oxygen species in HIF-1α protein levels in MIN6 cells under mildly hypoxic conditions, the cells were treated with antioxidants, such as *N*-acetyl-L-cysteine or Trolox (supplemental Fig. 1*b*). Because HIF-1α levels did not change after treatment with these antioxidants, contributions of reactive oxygen species, if any, were subtle. These results also confirmed that MIN6 cells become hypoxic more easily than PANC-1 cells.

Western Blotting Was Useful for Detecting Pimonidazole Adduct in Vitro and in Vivo—Next, pimonidazole adduct formation was assessed by Western blotting. When lysates of MIN6 cells in Fig. 1*a* were subjected to Western blotting, multiple bands were detected, consistent with the nature of pimonidazole, which nonspecifically forms adduct with molecules in the cells (Fig. 2*a*). As observed in Fig. 1, the intensity of Western blotting was inversely correlated with the oxygen tension. The intensity of the bands was higher in MIN6 cells than in PANC-1 cells at each oxygen tension examined. It should be noted that Western blotting was more sensitive than immunocytochemistry because the bands were detectable at higher oxygen tension. Because the islets in diabetes mice were suggested to be hypoxic (28), we applied Western blotting to the islets *in vivo* to detect pimonidazole adduct formation (Fig. 2, *b–e*). The pimonidazole adduct in the islets was remarkably increased in two different model mice of diabetes, KK-Ay (Fig. 2*b*) and ob/ob (Fig. 2*d*), compared with respective C57BL/6 control mice matched in age and sex. Quantification analysis revealed that the increase of adduct formation was statistically significant in KK-Ay (Fig. 2*c*) and ob/ob (Fig. 2*e*), whether glucose was loaded or not. Immunohistochemical analysis failed to detect pimonidazole adduct not only in pancreatic islet cells but also in other types of cells, including $CD31^+$ blood vessels (supplemental Fig. 2). Blood glucose concentrations of diabetic mice were higher than in control mice (supplemental Fig. 3*a*). Because high levels of blood glucose *per se* might affect the pimonidazole adduct formation in the islets, non-diabetic control mice were injected with glucose at 4 g/kg. Although blood glucose levels at 30 min after the glucose load increased more than 600 mg/dl, we did not observe the difference in pimonidazole adduct formation between saline- and glucose-loaded mice (supplemental Fig. 3, *b* and *c*), suggesting that pimonidazole adduct formation in islets is not accelerated solely by blood glucose levels.

As Mitochondrial Respiration Increased, MIN6 Cells Became Hypoxic—To examine the contributions of mitochondrial respiration on the generation of cellular hypoxia, we applied inhibitors of the respiratory chain, such as rotenone (an inhibitor of complex I) and antimycin A (an inhibitor of complex III). Decreased oxygen consumption was confirmed in the cells treated with either of the inhibitors (Fig. 3*a*).. The pimonidazole adduct in MIN6 cells at 3% oxygen tension was remarkably

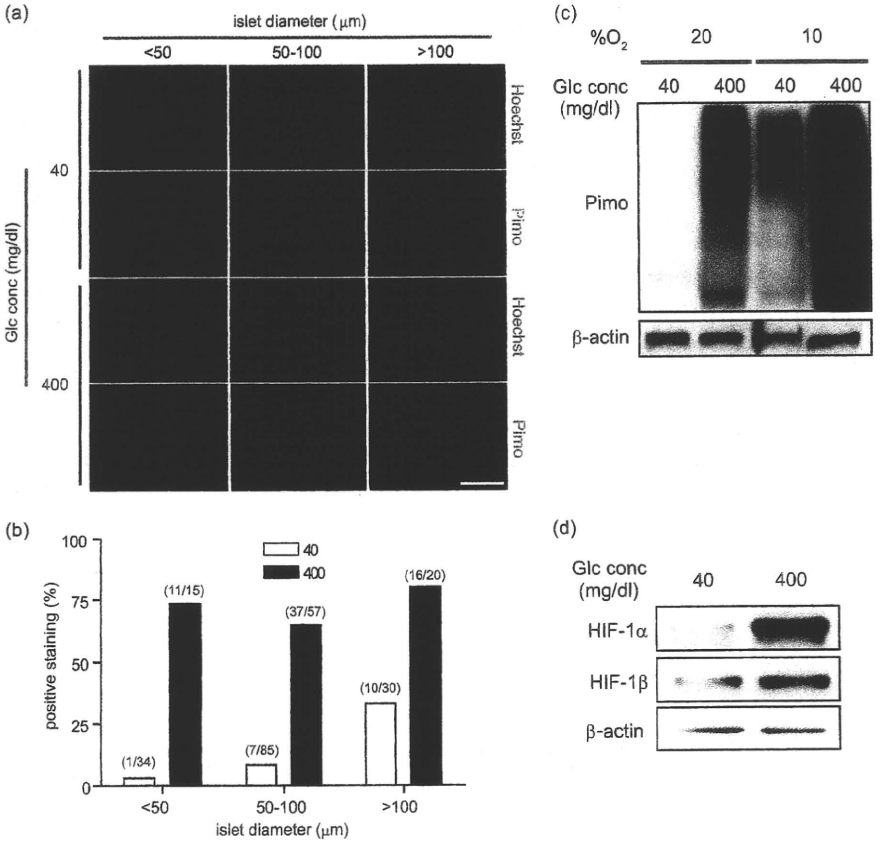

FIGURE 5. **Glucose-dependent cellular hypoxia in the cultured isolated islets *in vitro*.** *a*, immunohistochemistry of pimonidazole (*Pimo*) (*green*) and Hoechst 33342 (*Hoechst*) (*blue*) of isolated islets incubated with 40 or 400 mg/dl glucose at 20% oxygen tension for 1 h. Isolated islets were divided into three groups (<50, 50–100, and >100 μm) by their diameters. Representative images are shown. *Scale bar*, 100 μm. *b*, percentage of pimonidazole-positive ratio in the same conditions as in *a*. The islets incubated with 40 or 400 mg/dl glucose were represented as an *open bar* or *closed bar*, respectively. The number of the islets was indicated as (positive staining/total islets) above each bar. *c*, isolated islets incubated with 40 or 400 mg/dl glucose at 20 or 10% oxygen tension for 2 h were subjected to Western blotting for detection of pimonidazole adducts. Blotting of β-actin is shown as a loading control. *d*, expression levels of HIF-1α protein. Western blotting of HIF-1α and HIF-1β in the isolated islets cultured as in *c* is shown. Blotting of β-actin is shown as a loading control.

decreased by the inhibitor treatments (Fig. 3*b* and supplemental Fig. 4*a*). In addition, HIF-1α protein levels were strongly suppressed with rotenone and partially suppressed with antimycin A (Fig. 3*c*). The different potencies of the inhibitors in suppressing HIF-1α expression were consistent with previously reports (25). On the other hand, the uncouplers, such as carbonyl cyanide 4-phenylhydrazone and CCCP, have been reported to stimulate oxygen consumption through facilitating the proton influx into the mitochondrial matrix, bypassing ATP synthetase (29), which was confirmed in MIN6 cells (Fig. 3*a*). At 7% oxygen tension, where immunocytological staining of the pimonidazole adduct was barely detectable, the staining became detectable after treatment with CCCP (Fig. 3*d*). By flow cytometric analysis, a stronger signal was observed in CCCP-treated cells than in the non-treated cells under 7% oxygen (supplemental Fig. 4*b*). These results indicate that cellular hypoxia of MIN6 cells can be generated by intracellular oxygen consumption by mitochondrial respiration.

MIN6 Cells Became More Hypoxic by Glucose Stimulation—MIN6 cells consume oxygen when the cells secrete insulin in response to glucose stimulation (21). Mitochondrial oxidative phosphorylation is stimulated to fulfill the demand of ATP that is necessary for β-cell function (10). When MIN6 cells were exposed to elevated levels of glucose (400 mg/dl), insulin secretion increased 7-fold over the values obtained with 40 mg/dl glucose (Fig. 4*a*). We examined the change in oxygen consumption as a function of the glucose concentration of the medium. The oxygen consumption was higher when cells were cultured with higher concentrations of glucose (Fig. 4*b*). Furthermore, pimonidazole adduct formation was stronger at high glucose concentration than low concentration at 5% oxygen tension (Fig. 4*c*). Higher glucose concentrations yielded higher intensity of the HIF-1α band at 10% oxygen tension (Fig. 4*d*). Taken together, our data indicate that glucose-stimulated insulin secretion drove MIN6 cells into hypoxia.

Mouse Isolated Islets Became More Hypoxic by Glucose Stimulation—Because the behavior of MIN6 cells is known not to perfectly mimic primary β-cell physiology (30), we examined the islets isolated from mice and cultured *in vitro*. First, the islets were subjected to immunohistochemistry for detection of pimonidazole. In the islets cultured under normoxic conditions, more pimonidazole-positive islets were observed in samples stimulated by high glucose than in those cultured in low glucose medium, independent of the size of the islets (Fig. 5, *a* and *b*). Pimonidazole staining was rather homogenous in the high glucose-stimulated islets compared with that in the rela-

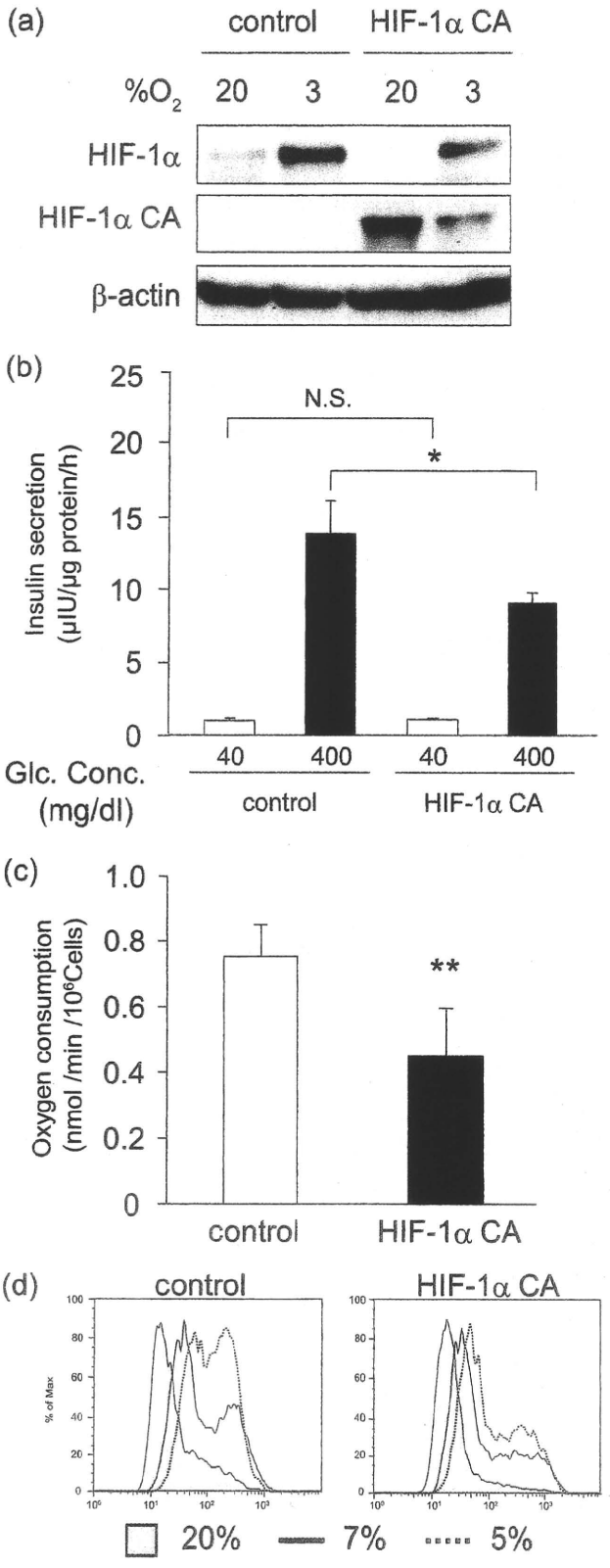

FIGURE 6. **Cellular hypoxia is attenuated in HIF-1α-overexpressing MIN6 cells.** *a*, generation of MIN6 cells carrying the constitutive active form of HIF-1α (HIF-1α CA). Control MIN6 cells and HIF-1α CA MIN6 cells were incubated at the indicated oxygen tension for 6 h, and the expression of endogenous as well as exogenous HIF-1α protein was assessed. Blotting of β-actin is shown as a loading control. *b*, impairment of insulin secretion in HIF-1α CA MIN6 cells. MIN6 cells were stimulated in a 40 and 400 mg/dl glucose concentration for 1 h, and insulin secretion was estimated as in Fig. 4*a*. *c*, decrease of oxygen consumption in HIF-1α CA MIN6 cells. The MIN6 cells were cultured in a 400 mg/dl glucose concentration, and oxygen consumption was measured. In *b* and *c*, the means ± S.D. (*error bars*) of values from each group are shown (*, $p > 0.05$; **, $p < 0.01$). *N.S.*, not significant. The experiments were repeated at least three times. *d*, cellular hypoxia is attenuated in HIF-1α CA5 MIN6 cells. Flow cytometric analysis of pimonidazole-stained cells at the indicated oxygen tensions is shown.

tively large islets in which pimonidazole staining was observed only in the core region, central staining (Fig. 5*a* and supplemental Fig. 5, *a* and *b*). Furthermore, Western blotting revealed that pimonidazole adduct was observed in the isolated islets stimulated by high glucose under normoxic conditions (Fig. 5*c*). When the islets were cultured under moderately hypoxic conditions, the pimonidazole adduct was observed even in the islets in low glucose medium, and more adduct was evident in the islets stimulated by high glucose levels. The expression levels of HIF-1α protein under the same conditions as in Fig. 5*c* were dramatically increased by treatment with high glucose, whereas HIF-1β expression was slightly increased (Fig. 5*d*). Thus, isolated islets became hypoxic when they were stimulated by high glucose.

HIF-1α Suppressed Insulin Secretion and Cellular Hypoxia Concurrently—Our observations that HIF-1α was induced in mild hypoxia in MIN6 cells prompted us to investigate the functional role of HIF-1α in the cellular hypoxia of MIN6 cells. We introduced the constitutively active form of HIF-1α, HIF-1α CA, into the MIN6 cells. HIF-1α CA proteins were confirmed to be expressed in HIF-1α CA cells even under normoxic conditions (Fig. 6*a*). In HIF-1α CA cells, the expression of *GLUT-1*, one of the HIF-1α target genes, was up-regulated (supplemental Fig. 6). Insulin secretion after glucose stimulation was impaired in HIF-1α CA cells (Fig. 6*b*), an outcome consistent with previous reports (28, 31, 32). Oxygen consumption was decreased in HIF-1α CA cells (Fig. 6*c*), and pimonidazole adduct formation under mildly hypoxic conditions was reduced in HIF-1α CA cells compared with control cells (Fig. 6*d*), findings that are consistent with the previous report using mouse embryonic fibroblasts (33). Thus, high levels of HIF-1α suppress insulin secretion and oxygen consumption, avoiding a decrease of the cellular oxygen levels in the insulin-secreting cells.

DISCUSSION

Pimonidazole is a derivative of 2-nitroimidazole, which forms adducts with intracellular macromolecules only at low oxygen tension (6). Nitroreductases within the cells transfer electrons to the parent compound and generate the nitro radical anion. Oxygen reoxidizes the nitro radical anion, thereby blocking further reduction of the parent compound. In the absence of oxygen, the nitro radical anion is further reduced and binds to -SH-containing molecules. The drawback of pimonidazole as a hypoxic marker is that it detects only severe hypoxia. Adduct formation of misonidazole, another 2-nitroimidazole derivative, steeply increases below partial oxygen pressure, 10 mm Hg (34).

On the other hand, the advantage of the pimonidazole detection is that it forms irreversible adducts under severely hypoxic conditions, so that the adduct formation serves as a record of the lowest oxygen tension to which cells have been exposed. The metabolic change following insulin secretion is transient and happens over a short time. The nature of irreversible adduct formation of pimonidazole is suitable to detect transient hypoxic events.

Formation of pimonidazole adduct is accelerated in reduced status. Thus, high levels of NADPH or glutathione might affect the adduct formation. Because glucose stimulation reportedly results in an increase of the NADPH/NADP+ ratio under normoxic conditions in islet β-cells (35), pimonidazole adduct formation is promoted not only by low oxygen tension but also possibly by an increase of the NADPH/$NADP^+$ ratio. Arteel *et al.* (36) reported that under hypoxic conditions, pimonidazole adduct formation mainly depends on oxygen tension rather than redox status. In addition, we did not observe an increase of pimonidazole adduct formation in normoxic MIN6 cells by glucose stimulation (Fig. 4*c*). Therefore, change of redox status by glucose stimulation might not be enough to increase pimonidazole adduct formation to the levels of our detection system. Thus, pimonidazole adduct formation is likely to reflect low oxygen tension in our experimental settings.

We demonstrated here that the pancreatic islet cells in two types of mouse diabetes model were hypoxic using Western blotting analysis. We failed to detect the signal by immunohistochemistry, indicating that Western blotting is more sensitive than immunostaining *in vivo*. It was previously suggested that the islet cells may be exposed to hypoxia in the progression of diabetes (28). Indeed, the hypoxia-related genes, including *HIF-1α*, *VEGF-A*, *PAI-1*, and *LDH-A*, are up-regulated in prediabetic ZDF, Zucker Diabetic Fatty, rat islets (37). The mechanism underlying islet cell hypoxia in the diabetes mice is not clear. Impairment of microcirculation and consequent decrease of blood supply might be a cause of islet hypoxia in these mice. Alternatively, as shown *in vitro* in this study, increased oxygen consumption by glucose stimulation is another possible cause. Further studies are needed to elucidate the mechanism.

There are two possibilities through which intracellular oxygen tension is decreased by acute oxygen consumption. One possibility is that intracellular hypoxia occurs secondary to pericellular hypoxia. Alternatively, intracellular hypoxia can occur despite the existence of adequate extracellular oxygen tension. Oxygen does not freely pass through the cellular membrane because oxygen diffusion is limited by the lipid bilayer (38). A water channel, aquaporin, is reportedly a gate for oxygen to enter into a cell (39). Therefore, cellular hypoxia can occur in those cells that consume large amounts of oxygen in a short period of time. These two possibilities are not mutually exclusive and can occur at the same time. It should be noted that the physiological oxygen tension of the normal tissue is between 24 and 66 mm Hg (3.3–9.2%) (6), which is often termed "moderately hypoxic" when the cells are cultured *in vitro*.

The islets of non-diabetic mice *in vivo* did not accumulate the pimonidazole adduct even after a challenge of high glucose (Fig. 2 and supplemental Fig. 3). In contrast, the isolated islets easily accumulated pimonidazole adduct when stimulated by high glucose (Fig. 5). Some protective mechanisms must exist to circumvent crisis *in vivo*, which might be impaired in the diabetic mice. The increase of blood flow by increased blood glucose levels can be a protective mechanism *in vivo* (40). High oxygen consumption due to the aerobic glucose metabolism of the isolated islets (41) might make the cellular hypoxia evident in the absence of the compensation mechanism.

The mice with the *Hif-1α* or *Hif-1β* deletion in β-cells showed impairment of glucose tolerance, not by the decrease of islet mass but by impaired insulin secretion of β-cells (42, 43). Lack of a hypoxia response mechanism might damage the islet cells over an extended time period. In MIN6 cells, we observed that basal as well as glucose-stimulated insulin secretion was intact under normoxic conditions when *Hif-1α* gene expression was suppressed,[3] an observation that supports the previous reports that the mice with *Hif-1α* deletion in β-cells do not show any defect in glucose homeostasis (28, 31).

Our data demonstrate that high glucose is a trigger of cellular hypoxia of pancreatic β-cells *in vitro*. In developing type 2 diabetes, blood glucose levels are elevated because of the peripheral glucose intolerance. In such a condition, the demand of the insulin secretion increases, and then the consequent increase of oxygen consumption might contribute to the β-cell hypoxia. Induction of HIF-1α by hypoxia might reduce insulin secretion, therefore suppressing the metabolic demand. Consequently, decreased oxygen consumption would offset severe cellular hypoxia in β-cells. Further investigation will be required to clarify whether islet hypoxia plays a role in deterioration of β-cell function in diabetes.

The findings here might also be applicable to islet transplantation. Preparing the intact islet from donors is one of the most important factors for the success of islet transplantation. During the process of islet isolation from donors and engraftment to recipients, hypoxia is a major cause of islet cell damage (44). Transiently reducing insulin secretion and consequent oxygen consumption might be beneficial for oxygenating the core hypoxic region of islets.

Acknowledgments—We thank Junichi Miyazaki for generously providing MIN6 cells and Toshiko Yasuda for secretarial support.

REFERENCES

1. Hochachka, P. W., and Somero, G. N. (2002) *Biochemical Adaptation*, Oxford University Press, New York
2. Semenza, G. L. (2000) *Genes Dev.* **14,** 1983–1991
3. Hagen, T., Taylor, C. T., Lam, F., and Moncada, S. (2003) *Science* **302,** 1975–1978
4. Doege, K., Heine, S., Jensen, I., Jelkmann, W., and Metzen, E. (2005) *Blood* **106,** 2311–2317
5. Semenza, G. L. (2007) *Science* **318,** 62–64
6. Höckel, M., and Vaupel, P. (2001) *J. Natl. Cancer. Inst.* **93,** 266–276
7. Zhdanov, A. V., Ward, M. W., Prehn, J. H., and Papkovsky, D. B. (2008) *J. Biol. Chem.* **283,** 5650–5661
8. Aragonés, J., Schneider, M., Van Geyte, K., Fraisl, P., Dresselaers, T., Mazzone, M., Dirkx, R., Zacchigna, S., Lemieux, H., Jeoung, N. H., Lambrechts, D., Bishop, T., Lafuste, P., Diez-Juan, A., Harten, S. K., Van Noten, P., De

[3] Y. Sato and M. Inoue, unpublished data.

Bock, K., Willam, C., Tjwa, M., Grosfeld, A., Navet, R., Moons, L., Vandendriessche, T., Deroose, C., Wijeyekoon, B., Nuyts, J., Jordan, B., Silasi-Mansat, R., Lupu, F., Dewerchin, M., Pugh, C., Salmon, P., Mortelmans, L., Gallez, B., Gorus, F., Buyse, J., Sluse, F., Harris, R. A., Gnaiger, E., Hespel, P., Van Hecke, P., Schuit, F., Van Veldhoven, P., Ratcliffe, P., Baes, M., Maxwell, P., and Carmeliet, P. (2008) *Nat. Genet.* **40,** 170–180

9. O'Hagan, K. A., Cocchiglia, S., Zhdanov, A. V., Tambawala, M. M., Cummins, E. P., Monfared, M., Agbor, T. A., Garvey, J. F., Papkovsky, D. B., Taylor, C. T., and Allan, B. B. (2009) *Proc. Natl. Acad. Sci. U.S.A.* **106,** 2188–2193
10. Wiederkehr, A., and Wollheim, C. B. (2006) *Endocrinology* **147,** 2643–2649
11. Jensen, M. V., Joseph, J. W., Ronnebaum, S. M., Burgess, S. C., Sherry, A. D., and Newgard, C. B. (2008) *Am. J. Physiol. Endocrinol Metab.* **295,** E1287–E1297
12. Eliasson, L., Abdulkader, F., Braun, M., Galvanovskis, J., Hoppa, M. B., and Rorsman, P. (2008) *J. Physiol.* **586,** 3313–3324
13. Maechler, P., and Wollheim, C. B. (2001) *Nature* **414,** 807–812
14. Miyazaki, J., Araki, K., Yamato, E., Ikegami, H., Asano, T., Shibasaki, Y., Oka, Y., and Yamamura, K. (1990) *Endocrinology* **127,** 126–132
15. Guppy, M., Kong, S. E., Niu, X., Busfield, S., and Klinken, S. P. (1997) *J. Cell. Physiol.* **170,** 1–7
16. Mukai, M., Kusama, T., Hamanaka, Y., Koga, T., Endo, H., Tatsuta, M., and Inoue, M. (2005) *Cancer Res.* **65,** 9121–9125
17. Okuyama, H., Krishnamachary, B., Zhou, Y. F., Nagasawa, H., Bosch-Marce, M., and Semenza, G. L. (2006) *J. Biol. Chem.* **281,** 15554–15563
18. Endo, H., Murata, K., Mukai, M., Ishikawa, O., and Inoue, M. (2007) *Cancer Res.* **67,** 8095–8103
19. Fukui, K., Yang, Q., Cao, Y., Takahashi, N., Hatakeyama, H., Wang, H., Wada, J., Zhang, Y., Marselli, L., Nammo, T., Yoneda, K., Onishi, M., Higashiyama, S., Matsuzawa, Y., Gonzalez, F. J., Weir, G. C., Kasai, H., Shimomura, I., Miyagawa, J., Wollheim, C. B., and Yamagata, K. (2005) *Cell. Metab.* **2,** 373–384
20. He, F., Deng, X., Wen, B., Liu, Y., Sun, X., Xing, L., Minami, A., Huang, Y., Chen, Q., Zanzonico, P. B., Ling, C. C., and Li, G. C. (2008) *Cancer Res.* **68,** 8597–8606
21. Soejima, A., Inoue, K., Takai, D., Kaneko, M., Ishihara, H., Oka, Y., and Hayashi, J. I. (1996) *J. Biol. Chem.* **271,** 26194–26199
22. Wang, W., Upshaw, L., Strong, D. M., Robertson, R. P., and Reems, J. (2005) *J. Endocrinol.* **185,** 445–455
23. Gilbert, M., Jung, S. R., Reed, B. J., and Sweet, I. R. (2008) *J. Biol. Chem.* **283,** 24334–24342
24. Bracken, C. P., Fedele, A. O., Linke, S., Balrak, W., Lisy, K., Whitelaw, M. L., and Peet, D. J. (2006) *J. Biol. Chem.* **281,** 22575–22585
25. Brown, S. T., and Nurse, C. A. (2008) *Am. J. Physiol.* **294,** C1305–C1312
26. Brunelle, J. K., Bell, E. L., Quesada, N. M., Vercauteren, K., Tiranti, V., Zeviani, M., Scarpulla, R. C., and Chandel, N. S. (2005) *Cell. Metab.* **1,** 409–414
27. Guzy, R. D., Hoyos, B., Robin, E., Chen, H., Liu, L., Mansfield, K. D., Simon, M. C., Hammerling, U., and Schumacker, P. T. (2005) *Cell. Metab.* **1,** 401–408
28. Zehetner, J., Danzer, C., Collins, S., Eckhardt, K., Gerber, P. A., Ballschmieter, P., Galvanovskis, J., Shimomura, K., Ashcroft, F. M., Thorens, B., Rorsman, P., and Krek, W. (2008) *Genes Dev.* **22,** 3135–3146
29. Daunt, M., Dale, O., and Smith, P. A. (2006) *Endocrinology* **147,** 1527–1535
30. Poitout, V., Olson, L. K., and Robertson, R. P. (1996) *Diabetes Metab.* **22,** 7–14
31. Cantley, J., Selman, C., Shukla, D., Abramov, A. Y., Forstreuter, F., Esteban, M. A., Claret, M., Lingard, S. J., Clements, M., Harten, S. K., Asare-Anane, H., Batterham, R. L., Herrera, P. L., Persaud, S. J., Duchen, M. R., Maxwell, P. H., and Withers, D. J. (2009) *J. Clin. Invest.* **119,** 125–135
32. Puri, S., Cano, D. A., and Hebrok, M. (2009) *Diabetes* **58,** 433–441
33. Papandreou, I., Cairns, R. A., Fontana, L., Lim, A. L., and Denko, N. C. (2006) *Cell. Metab.* **3,** 187–197
34. Gross, M. W., Karbach, U., Groebe, K., Franko, A. J., and Mueller-Klieser, W. (1995) *Int. J. Cancer* **61,** 567–573
35. Ivarsson, R., Quintens, R., Dejonghe, S., Tsukamoto, K., in 't Veld, P., Renström, E., and Schuit, F. C. (2005) *Diabetes* **54,** 2132–2142
36. Arteel, G. E., Thurman, R. G., and Raleigh, J. A. (1998) *Eur. J. Biochem.* **253,** 743–750
37. Li, X., Zhang, L., Meshinchi, S., Dias-Leme, C., Raffin, D., Johnson, J. D., Treutelaar, M. K., and Burant, C. F. (2006) *Diabetes* **55,** 2965–2973
38. Ivanov, I. I., Fedorov, G. E., Gus'kova, R. A., Ivanov, K. I., and Rubin, A. B. (2004) *Biochem. Biophys. Res. Commun.* **322,** 746–750
39. Echevarría, M., Muñoz-Cabello, A. M., Sánchez-Silva, R., Toledo-Aral, J. J., and López-Barneo, J. (2007) *J. Biol. Chem.* **282,** 30207–30215
40. Jansson, L., and Hellerström, C. (1986) *Am. J. Physiol.* **251,** E644–E647
41. Schuit, F., De Vos, A., Farfari, S., Moens, K., Pipeleers, D., Brun, T., and Prentki, M. (1997) *J. Biol. Chem.* **272,** 18572–18579
42. Cheng, K., Ho, K., Stokes, R., Scott, C., Lau, S. M., Hawthorne, W. J., O'Connell, P. J., Loudovaris, T., Kay, T. W., Kulkarni, R. N., Okada, T., Wang, X. L., Yim, S. H., Shah, Y., Grey, S. T., Biankin, A. V., Kench, J. G., Laybutt, D. R., Gonzalez, F. J., Kahn, C. R., and Gunton, J. E. (2010) *J. Clin. Invest.* **120,** 2171–2183
43. Gunton, J. E., Kulkarni, R. N., Yim, S., Okada, T., Hawthorne, W. J., Tseng, Y. H., Roberson, R. S., Ricordi, C., O'Connell, P. J., Gonzalez, F. J., and Kahn, C. R. (2005) *Cell* **122,** 337–349
44. Miao, G., Ostrowski, R. P., Mace, J., Hough, J., Hopper, A., Peverini, R., Chinnock, R., Zhang, J., and Hathout, E. (2006) *Am. J. Transplant.* **6,** 2636–2643

Biochemical and Biophysical Research Communications 407 (2011) 620–625

Contents lists available at ScienceDirect

Biochemical and Biophysical Research Communications

journal homepage: www.elsevier.com/locate/ybbrc

Voltage-gated K^+ channel KCNQ1 regulates insulin secretion in MIN6 β-cell line

Kazuya Yamagata [a,*], Takafumi Senokuchi [a], Meihong Lu [b], Makoto Takemoto [b], Md. Fazlul Karim [a], Chisa Go [a], Yoshifumi Sato [a], Mitsutoki Hatta [a], Tatsuya Yoshizawa [a], Eiichi Araki [c], Junichi Miyazaki [d], Wen-Jie Song [b]

[a] Department of Medical Biochemistry, Faculty of Life Sciences, Kumamoto University, 1-1-1 Honjo, Kumamoto 860 8556, Japan
[b] Department of Sensory and Cognitive Physiology, Faculty of Life Sciences, Kumamoto University, Kumamoto, Japan
[c] Department of Metabolic Medicine, Faculty of Life Sciences, Kumamoto University, Kumamoto, Japan
[d] Division of Stem Cell Regulation Research, Osaka University Graduate School of Medicine, Osaka, Japan

ARTICLE INFO

Article history:
Received 15 March 2011
Available online 21 March 2011

Keywords:
Type 2 diabetes
Gene
KCNQ1
Insulin secretion

ABSTRACT

KCNQ1, located on 11p15.5, encodes a voltage-gated K^+ channel with six transmembrane regions, and loss-of-function mutations in the KCNQ1 gene cause hereditary long QT syndrome. Recent genetic studies have identified that single nucleotide polymorphisms located in intron 15 of the KCNQ1 gene are strongly associated with type 2 diabetes and impaired insulin secretion. In order to understand the role of KCNQ1 in insulin secretion, we introduced KCNQ1 into the MIN6 mouse β-cell line using a retrovirus-mediated gene transfer system. In KCNQ1 transferred MIN6 cells, both the density of the KCNQ1 current and the density of the total K^+ current were significantly increased. In addition, insulin secretion by glucose, pyruvate, or tolbutamide was significantly impaired by KCNQ1-overexpressing MIN6 cells. These results suggest that increased KCNQ1 protein expression limits insulin secretion from pancreatic β-cells by regulating the potassium channel current.

1. Introduction

KCNQ1, located on 11p15.5, encodes a voltage-gated K^+ channel with six transmembrane regions and is expressed in the heart, stomach, small and large intestine, kidney and pancreas [1]. In cardiac myocytes, KCNQ1 and the regulatory subunit KCNE1 assemble to form a slowly activating cardiac potassium channel (I_{Ks}) [2,3]. This channel contributes to the delayed outwardly rectifying K^+ current, and loss-of-function mutations in the KCNQ1 gene cause hereditary long QT syndrome due to the reduction of the repolarizing potassium cardiac current I_{Ks} [4,5].

Two recent independent genome-wide association studies (GWAS) identified that single nucleotide polymorphisms (SNPs) located in intron 15 of the KCNQ1 gene (e.g. rs2237892, rs2237895, and rs2237897) are strongly associated with type 2 diabetes [6,7]. Genetic studies also have revealed that the risk alleles of the KCNQ1 gene are associated with impaired insulin secretion rather than insulin resistance [6,8,9], suggesting the important role of KCNQ1 in insulin secretion by pancreatic β-cells. Although the molecular mechanism of how KCNQ1 SNPs within the intron affects insulin secretion is unclear, it is plausible that the polymorphisms alter the expression of the KCNQ1 gene in β-cells. Increased KCNQ1 function would impair insulin secretion by causing premature repolarization of the action potential. Indeed, KCNQ1 is expressed in insulin-secreting INS-1 β-cells, and inhibition of KCNQ1 channel activity by a selective inhibitor chromanol 293B significantly increased insulin secretion by INS-1 cells [10]. Hence, we expect that increased KCNQ1 gene expression in pancreatic β-cells is probably responsible for the insulin secretion defect, but this hypothesis has not been verified so far.

In order to understand the role of KCNQ1 in insulin secretion, we introduced KCNQ1 into the MIN6 mouse β-cell line using a retrovirus-mediated gene transfer system. In KCNQ1-transferred MIN6 cells, the density of the 293B-sensitive KCNQ1 current was significantly increased and insulin secretion by glucose, pyruvate, or tolbutamide was significantly impaired. These results indicate that KCNQ1 expression plays an important role in insulin secretion by pancreatic β-cells.

2. Methods

2.1. Cell culture

The pancreatic β-cell line MIN6 was maintained in Dulbecco's modified Eagles' medium (DMEM) (25 mM glucose) containing 10% (v/v) fetal bovine serum, 1% (v/v) penicillin/streptomycin, and 100 μM β-mercaptoethanol (β-ME) and incubated at 37 °C in 5% CO_2 [11]. Plat-E retrovirus packaging cells were maintained in DMEM containing 10% (v/v) fetal bovine serum [12].

* Corresponding author. Fax: +81 96 364 6940.
E-mail address: k-yamaga@kumamoto-u.ac.jp (K. Yamagata).

0006-291X/$ - see front matter © 2011 Elsevier Inc. All rights reserved.
doi:10.1016/j.bbrc.2011.03.083

2.2. Isolation of pancreatic islets

Pancreatic islets were isolated from C57BL/6 mice by the collagenase digestion method as described previously [13].

2.3. Reverse transcription-PCR

Total RNA was isolated from MIN6 cells and mouse pancreatic islets using Sepasol RNA I Super G reagent (Nacalai Tesque, Kyoto, Japan). cDNA synthesis was performed with 1 μg total RNA using a PrimeScript RT reagent kit (Takara, Tokyo, Japan). The following primers were used for specific amplification of mouse KCNQ1: 5′-TGCTCGGAGTCACACGCTTC-3′ and 5′-TCCAGGTCCAGGTCCTCTGC-3′ (product size 279 bp) and mouse TBP: 5′-CCCCTTGTACCCTTCACCAAT-3′ and 5′-GAAGCTGCGGTACAATTCCAG-3′ (product size 89 bp).

2.4. Retrovirus infection

Mouse KCNQ1 cDNA clone (IMAGE 6397978) was purchased from Invitrogen (Carlsbad, CA). The entire coding region with 60 and 939 nucleotides of the 5′ and 3′ untranslated region, respectively, was subcloned into pMXs-puro retrovirus vector [14]. The construct was verified by sequencing. For the production of retroviruses, pMXs-KCNQ1 and empty pMXs vectors were transfected into Plat-E cells using FuGENE6 (Roche Applied Science, Mannheim, Germany). MIN6 cells were infected with the retroviruses and selected with puromycin (5 μg/ml) [15].

2.5. Western blot analysis

MIN6 cells were directly lysed in SDS sample buffer (10 mM Tris (pH 6.8), 6% (w/v) urea, 1% (v/v) SDS, 3.3% (v/v) glycerol, 0.13 M β-ME, and 0.005% (w/v) BPB). After incubation for 3 h at 4 °C with gentle shaking, lysates were centrifuged at 10,000×*g* for 15 min. The lysates were not subjected to heat treatment prior to Western blot analysis to avoid aggregation and degradation. Western blotting was performed as previously described [16] using the primary antibody against KCNQ1 (1:200; Sigma, P5372) and β-actin (1:5000; Sigma, AC-15).

2.6. Immunocytochemistry

MIN6 cells were fixed in 4% paraformaldehyde in 0.1 M phosphate buffer for 20 min at room temperature (RT). After washing in phosphate-buffered saline (PBS), the cells were treated with 5% normal donkey serum in PBS, containing 0.1% (v/v) Triton X-100 for 1 h at RT. The cells were then incubated with a goat anti-KCNQ1 antibody (1:200; Santa Cruz Biotechnology, Santa Cruz, CA, USA, sc-10646) overnight at 4 °C. After washing in PBS with 0.1% Triton X-100, the cells were incubated with an Alexa Fluor 488-conjugated donkey anti-goat IgG (1:500; Invitrogen, A11055) for 1.5 h at RT, followed by counterstaining with DAPI.

2.7. Recording of potassium currents

Whole cell recordings of K^+ currents were obtained using techniques described previously [17]. Briefly, cells were perfused in a background solution consisting of (in mM) 140 NaCl, 5 glucose, 15 Hepes, 2 KCl, 2 $MgCl_2$, and 1 $CaCl_2$ (pH 7.4 adjusted with NaOH, 300 ± 5 mOsm/l). The external solution consisted of (in mM) 140 NaCl, 5 KCl, 2 $MgCl_2$, 10 Hepes, and 5 glucose (pH 7.4 adjusted with NaOH, 300 ± 5 mOsm/l). KCNQ1 current was defined as the current blocked by 293B (100 μM; Sigma) [10]. Recording pipettes were filled with (in mM) 120 potassium gluconate, 3 $MgCl_2$, 10 Hepes, 10 EGTA, 12 phosphocreatine, 2 ATP, and 0.2 GTP (pH 7.2–7.3 adjusted with NaOH, 280 ± 5 mOsm/l). Recordings were obtained using an Axon Instrument 200B patch-clamp amplifier and were controlled and monitored by a PC running pClamp 7.0. After seal rupture, series resistance was compensated 70–90%. Current density was calculated by dividing current amplitude with whole-cell capacitance, which reflects the cell surface area.

2.8. Insulin secretion and insulin content

After reaching 80% confluence, MIN6 cells were plated in 24-well plates at a density of 3×10^5 cells per well. After 72 h, cells were preincubated at 37 °C for 60 min in Hepes–Krebs buffer (in mM) (118.4 NaCl, 4.7 KCl, 1.2 KH_2PO_4, 2.4 $CaCl_2$, 1.2 $MgSO_4$, 20 $NaHCO_3$, 3 glucose, and 10 Hepes) containing 0.5% (w/v) bovine serum albumin (BSA). MIN6 cells were then incubated for 60 min in Hepes–Krebs buffer containing 20 mM glucose (in the presence or absence of 100 nM GLP-1 (Peptide Institute, Japan), 20 mM pyruvate, or 500 μM tobutamide. Insulin was measured by using a mouse insulin ELISA kit (AKRIN-011T; Shibayagi, Japan). The insulin content was determined after extraction with acid ethanol as described previously [18].

2.9. Statistical analysis

Values are expressed as the mean ± SD. Statistical significance was tested using two-tailed Student's *t*-test or the non-parametric Mann–Whitney *U* test (for electrophysiological experiments). A *p* value less than 0.05 was considered significant.

3. Results

3.1. Retrovirus-mediated expression of KCNQ1 in MIN6 cells

KCNQ1 mRNA was previously shown to be expressed in mouse pancreatic islets and insulin-secreting INS-1 cells [6,10]. Using reverse transcription-PCR, we confirmed the expression of KCNQ1 mRNA in MIN6 β-cells (Fig. 1A). To elucidate the function of KCNQ1 in pancreatic β-cells, we first obtained MIN6 cells stably overexpressing KCNQ1 (KCNQ1-MIN6 cells) and control MIN6 cells (pMX-MIN6 cells) by retrovirus infection. KCNQ1 protein expression in control pMX-MIN6 cells was below the detection level of Western blotting. In contrast, strong expression of the channel protein (75 kDa) was detected in KCNQ1-MIN6 cells by Western blotting (Fig. 1B). Immunohistochemical analysis also revealed elevated levels of KCNQ1 protein in most KCNQ1-MIN6 cells (Fig. 1C–E). KCNQ1 is a membrane protein and functions as a voltage-gated potassium channel on the plasma membrane [19]. We next examined the subcellular localization of KCNQ1 protein with a confocal microscope. As shown in Fig. 1I, KCNQ1 expression was largely localized to the cytoplasmic membrane of KCNQ1-MIN6 cells.

3.2. Electrophysiology of KCNQ1-MIN6 cells

To test whether retroviral infection of KCNQ1 alters the function of K^+ channels, we made whole-cell recordings of depolarization-activated K^+ currents from KCNQ1-MIN6 as well as pMX-MIN6 cells. First, we examined the voltage dependence of K^+ conductance using voltage steps from −60 mV to +50 mV (Fig. 2A). Activation curves were obtained by fitting the tail current (Fig. 2A, arrow) with a Boltzmann function (Fig. 2B) [20]. The half-activation voltage was 2.23 ± 2.05 mV ($n = 12$) in KCNQ1-MIN6 cells, which is decreased, but not significantly different from that in pMX-MIN6 cells (3.07 ± 1.93 mV, $n = 13$). The slope factor in KCNQ1-MIN6 cells, however, was significantly larger than in con-

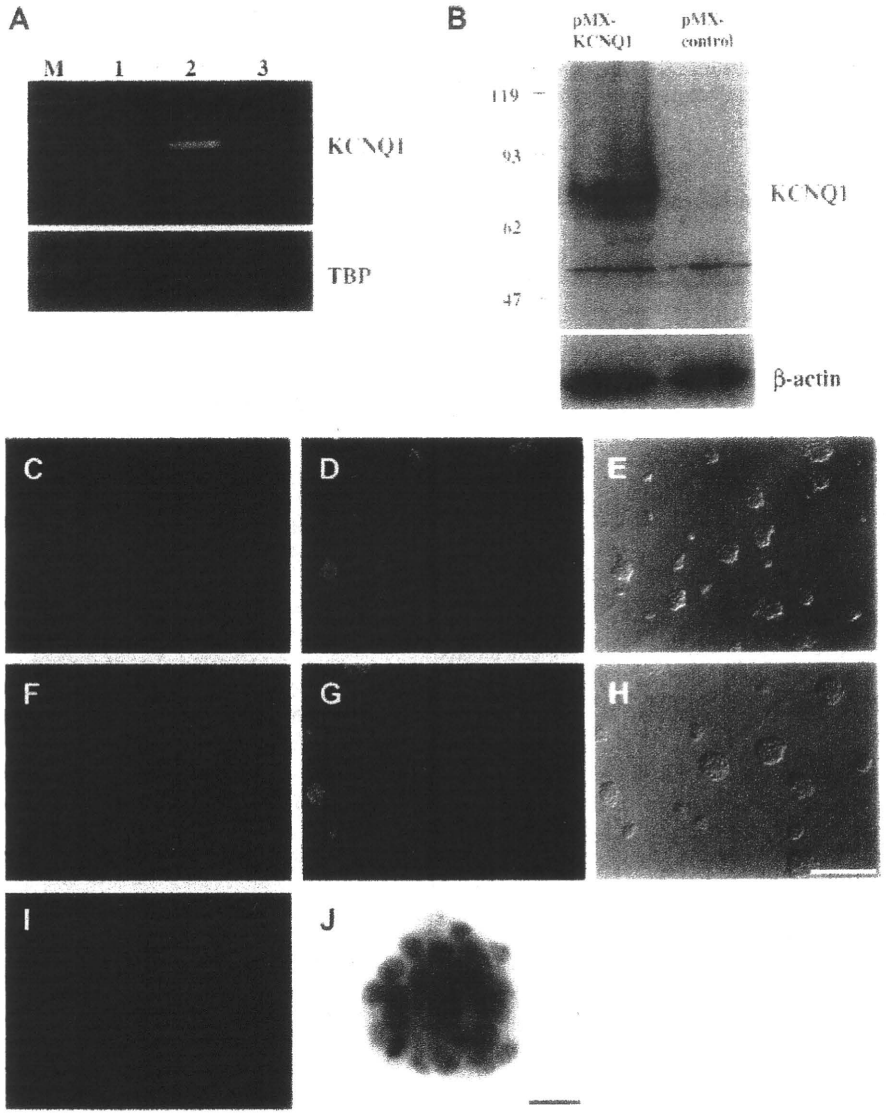

Fig. 1. Expression of KCNQ1 in MIN6 cells. (A) Reverse transcription-PCR analysis of KCNQ1 and TBP. RNA was extracted from mouse pancreatic islets (lane 2) and MIN6 cells (lane 3). No products were amplified in the absence of cDNA (lane 1). (B) Western blot analysis of KCNQ1 and β-actin protein levels in pMX-KCNQ1 and pMX-MIN6 cells. (C–I) Immunohistochemical analysis of KCNQ1 expression in KCNQ1-MIN6 (C–E) and pMX-MIN6 cells (F–H). MIN6 cells were stained with anti-KCNQ1 antibody (C, F) and DAPI (D, G). Cells were photographed with the same exposure time. Intracellular localization of KCNQ1 in KCNQ1-MIN6 cells (I). Note the intense signal at the cytoplasmic membrane. Moderate signals were also found in the cytoplasm. (J) DAPI staining of the same aggregate in I. Scale bars: 0.2 mm (C–H), 20 μm (I, J).

trol cells (14.20 ± 0.80 mV vs. 11.57 ± 0.74; Fig. 2B, inset). This significant increase in slope factor, together with the decrease in the mean value of half activation, resulted in more activation in KCNQ1-MIN6 cells in the voltage range from approximately −50 mV to 0 mV. Nevertheless, a voltage step to + 40 mV activated the near-maximum conductance in both KCNQ1-MIN6 and control cells (Fig. 2B). We thus estimated K^+ conductance in KCNQ1-MIN6 cells and pMX-MIN6 cells using a single voltage step to +40 mV. Fig. 2C and D show examples of such recordings. KCNQ1 currents were isolated by subtracting the current after 293B application from the control potassium currents (Fig. 2C and D) [10]. KCNQ1 currents were observed in both KCNQ1-MIN6 and control MIN6 cells. The currents peaked rapidly and then inactivated slowly (Fig. 2C and D), suggesting the homomeric nature of KCNQ1 channels in these cells [2,3]. As shown in Fig. 2E, the density of 293B-sensitive current increased significantly in KCNQ1-MIN6 cells ($p < 0.05$). This increase also resulted in a significant increase in the average value of the density of total K^+ currents in KCNQ1-MIN6 cells ($p < 0.05$, Fig. 2F).

3.3. Insulin secretion by KCNQ1-MIN6 cells

In β-cells, an increase of the ATP/ADP ratio due to glucose metabolism closes the ATP-sensitive potassium (K_{ATP}) channel, leading to membrane depolarization, calcium influx, and insulin exocytosis. Also, upon membrane depolarization, voltage-dependent K^+ channels open to repolarize the action potential, and limit insulin secretion [21]. Since the density of 293B-sensitive KCNQ1 and total K^+ currents was significantly increased in KCNQ1-MIN6 cells, we examined insulin secretion from the cells. KCNQ1-MIN6 cells and control pMX-MIN6 cells were incubated with 3 mM and 20 mM glucose. Insulin secretion from KCNQ1-MIN6 cells by high glucose was significantly decreased (28.3% of control, $p < 0.01$) compared with that from control cells (Fig. 3A).

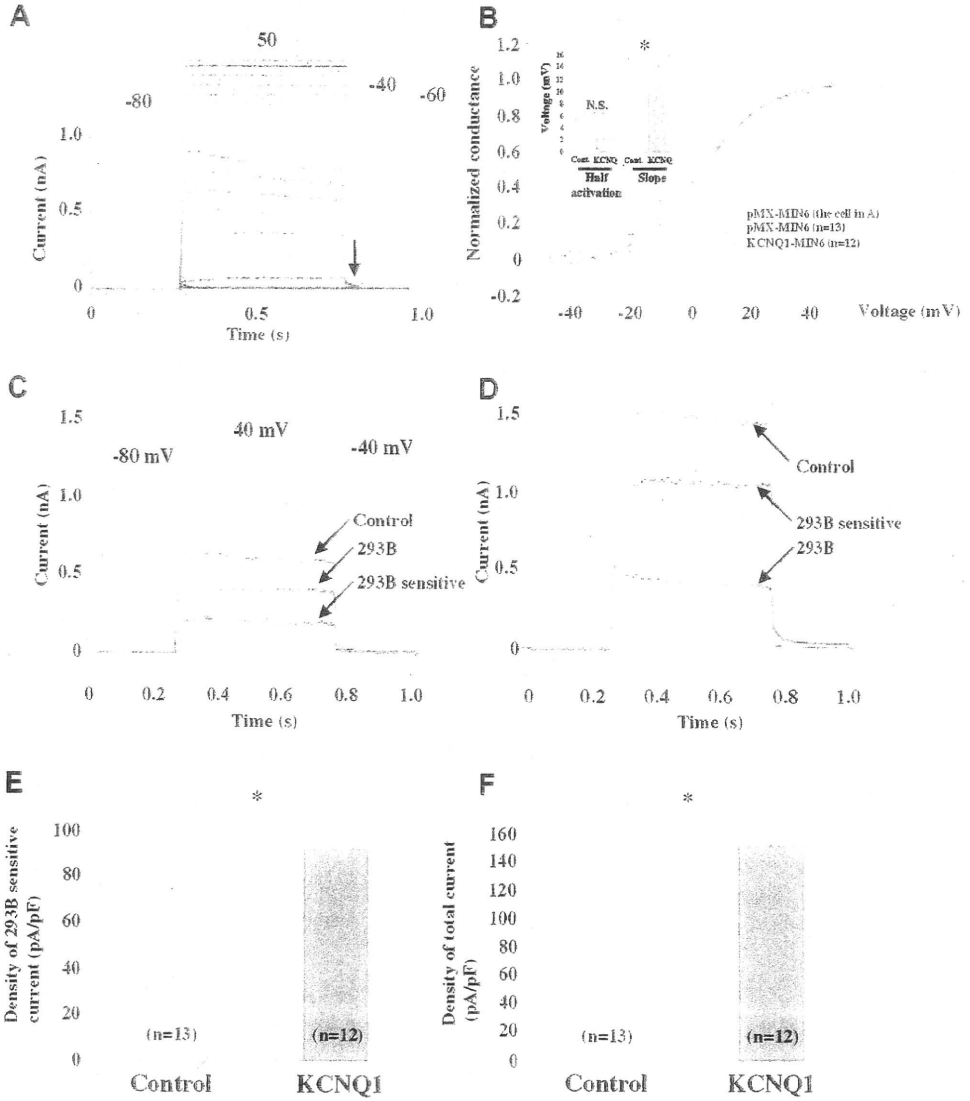

Fig. 2. Increased KCNQ1 current density and total potassium current density in KCNQ1-MIN6 cells. (A) K^+ current evoked with the voltage steps shown in the upper panel in a control pMX-MIN6 cell. Channel activation curves were constructed using the tail currents (arrow). (B) Channel activation curves. Diamond symbols represent data from the cell in A. Circles represent the data from a group of pMX-MIN6 cells ($n = 13$), and squares show the data from a group of KCNQ1-MIN6 cells ($n = 12$). Curves are Boltzmann fitting curves for each group of data. Inset: histograms showing the values of channel half-activation and slope factor. The slope in KCNQ1-MIN6 cells was significantly larger than in control cells ($p < 0.05$). (C) Representative recordings from a pMX-MIN6 cell. K^+ current was evoked with voltage steps to +40 mV from a −80 mV prepulse. KCNQ1 current was isolated by subtracting the current after application of 293 B from the control current. (D) Representative currents from a KCNQ1-MIN6 cell, evoked using the same voltage protocol as in C. (E) Density of KCNQ1 current in KCNQ1- and pMX-MIN6 cells. $^*p < 0.05$. (F) Density of total K^+ current in infected and uninfected cells. $^*p < 0.05$.

KCNQ1 overexpression also affected insulin secretion at low glucose concentration (decreased by 42.5%, $p < 0.05$) in KCNQ1-MIN6 cells. The reduction of insulin secretion was not due to altered insulin synthesis since the insulin content of KCNQ1-MIN6 cells and control MIN6 cells was similar (Fig. 3B). Glucose is metabolized to pyruvate through glycolysis. Pyruvate-induced insulin secretion was also significantly reduced in KCNQ1-MIN6 cells (39.4% of control, $p < 0.01$). Tolbutamide stimulates insulin secretion by blocking the K_{ATP} channel. As was the case for glucose, insulin response to tolbutamide was also significantly inhibited (51.8% of control, $p < 0.01$) in KCNQ1-MIN6 cells. Mannose is metabolized to fructose 6-phosphate and enters glycolysis [22]. Insulin secretion by 20 mM mannose was also decreased in KCNQ1-MIN6 cells compared to pMX-MIN6 cells (data not shown). These data clearly indicate that increased expression of KCNQ1 protein reduces insulin secretion by MIN6 cells.

Glucagon-like peptide-1 (GLP-1) potentiates insulin secretion from pancreatic β-cells by increasing intracellular cAMP concentration [23]. We next examined the insulinotropic action of GLP-1 in KCNQ1-MIN6 cells. In the presence of GLP-1, 20 mM glucose-stimulated insulin secretion from KCNQ1-MIN6 cells was significantly augmented by 2.2-fold (GLP-1(−): 192.4 ± 35.7 ng/mg protein/60 min, GLP-1(+): 427.9 ± 84.2 ng/mg protein/60 min, $p < 0.01$). These results suggest that GLP-1 can exert insulinotropic effects under the condition of enhanced membrane repolarization.

4. Discussion

Recent genetic studies have revealed that common genetic variations in the KCNQ1 gene is associated with type 2 diabetes and β-cell function [6–9]. KCNQ1 null mice have been reported to show

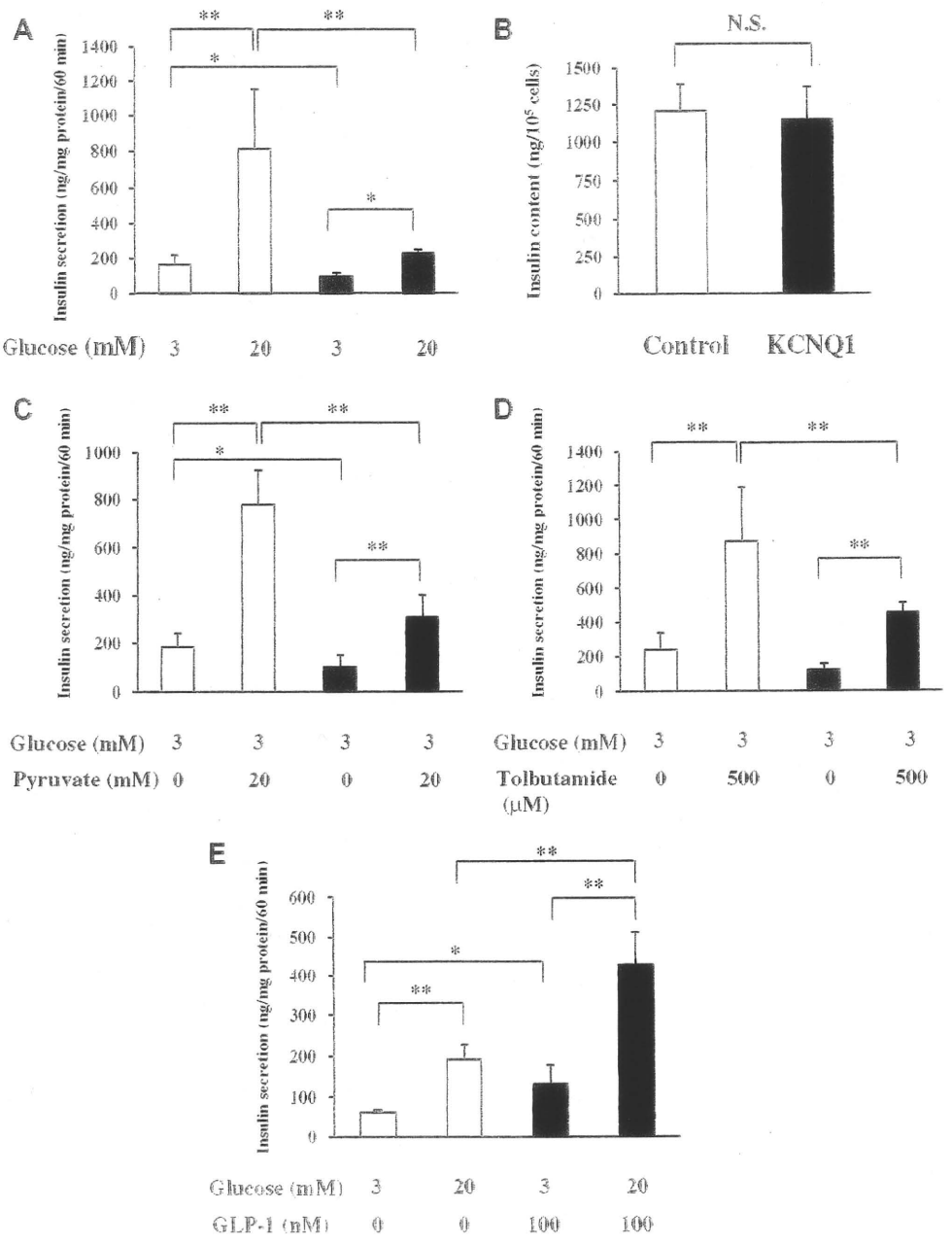

Fig. 3. Insulin secretory response to glucose (A), pyruvate (C), and tolbutamide (D) from pMX-MIN6 cells (open bars) and KCNQ1-MIN6 cells (solid bars). Data are the mean ± SD of 4–6 experiments. $^{*}p < 0.05$; $^{**}p < 0.01$. (B) Insulin content of KCNQ1-MIN6 cells and pMX-MIN6 cells ($n = 4$). NS, not significant. (E) Insulin release in response to 100 nM GLP-1 in KCNQ1-MIN6 cells ($n = 4$). $^{*}p < 0.05$; $^{**}p < 0.01$.

enhanced insulin sensitivity and improved glucose tolerance compared with the wild type [24]. However, the contribution of KCNQ1 to β-cell function is largely unknown. In cardiac myocytes, KCNQ1 associates with KCNE1 to form the I_{Ks} potassium current, which is characterized by slow activation kinetics and this current is critical for repolarization of the cardiac action potential [2,3]. The results presented here indicate that KCNQ1 current in both KCNQ1-MIN6 and control MIN6 cells is characterized by a rapid activation time course and a slow inactivation process, suggesting that KCNQ1 mainly functions without KCNE1 association in MIN6 cells. Recent studies have shown that KCNQ1 associates with the KCNE subunit (KCNE1–4), with different stoichiometries having different gating properties [25]. Although we did not directly test the expression of KCNE1–4 in MIN6 cells, no expression of KCNE1 was found in the INS-1 β-cell line by reverse transcription-PCR [10].

After KCNQ1 introduction, both changes in channel activation properties (more activation in the voltage range from −50 mV to 0 mV) and the increase in channel density (see Fig. 2) are expected to lower the rate of action potentials and thus decrease insulin release. Our *in vitro* results revealed that elevated expression of KCNQ1 in MIN6 cells indeed limits insulin secretion. Thus, we would expect that risk SNPs increase KCNQ1 expression in pancreatic β-cells and that enhanced KCNQ1 function is responsible for the development of type 2 diabetes; however, further experiments are necessary to examine the role of KCNQ1 *in vivo*. Analysis of

transgenic mice with pancreatic β-cell-targeted expression of KCNQ1 could be useful.

We also found that GLP-1 can compensate for the insulin secretion defect from KCNQ1-MIN6 cells. GLP-1 enhances insulin secretion through different mechanisms [23] and it has been reported that GLP-1 receptor activation antagonizes voltage-gated K^+ currents in rat β-cells [26]. Further studies are necessary to understand the role of GLP-1 in KCNQ1 channel in β-cells. GLP-1 analogues and inhibitors of dipeptidyl peptidase-4 (DPP-4), GLP-1 cleavage peptidase, are now widely used for the treatment of type 2 diabetes. Our results suggest that a therapeutic approach enhancing GLP-1 action would be beneficial to treat type 2 diabetes having risk SNPs of the KCNQ1 gene.

Acknowledgments

We thank Prof. T. Kitamura (Tokyo University) for providing the Plat-E cells and pMXs vector. This work was supported by grants from Japan Society for the Promotion of Science, Takeda Science Foundation, and Novo Nordisk Insulin Research Foundation.

References

[1] J. Robbins, KCNQ potassium channels: physiology, pathophysiology, and pharmacology, Pharmacol. Ther. 90 (2001) 1–19.
[2] J. Barhanin, F. Lesage, E. Guillemare, M. Fink, M. Lazdunski, G. Romey, K_VLQT1 and lsK (minK) proteins associate to form the I_{Ks} cardiac potassium current, Nature 384 (1996) 78–80.
[3] M.C. Sanguinetti, M.E. Curran, A. Zou, J. Shen, P.S. Spector, D.L. Atkinson, M.T. Keating, Coassembly of K_VLQT1 and minK (lsK) proteins to form cardiac I_{Ks} potassium channel, Nature 384 (1996) 80–83.
[4] Q. Wang, M.E. Curran, I. Splawski, T.C. Burn, J.M. Millholland, T.J. VanRaay, J. Shen, K.W. Timothy, G.M. Vincent, T. de Jager, P.J. Schwartz, J.A. Toubin, A.J. Moss, D.L. Atkinson, G.M. Landes, T.D. Connors, M.T. Keating, Positional cloning of a novel potassium channel gene: KVLQT1 mutations cause cardiac arrhythmias, Nat. Genet. 12 (1996) 17–23.
[5] N. Neyroud, F. Tesson, I. Denjoy, M. Leibovici, C. Donger, J. Barhanin, S. Fauré, F. Gary, P. Coumel, C. Petit, K. Schwartz, P. Guicheney, A novel mutation in the potassium channel gene KVLQT1 causes the Jervell and Lange-Nielsen cardioauditory syndrome, Nat. Genet. 15 (1997) 186–189.
[6] K. Yasuda, K. Miyake, Y. Horikawa, K. Hara, H. Osawa, H. Furuta, Y. Hirota, H. Mori, A. Jonsson, Y. Sato, K. Yamagata, Y. Hinokio, H.Y. Wang, T. Tanahashi, N. Nakamura, Y. Oka, N. Iwasaki, Y. Iwamoto, Y. Yamada, Y. Seino, H. Maegawa, A. Kashiwagi, J. Takeda, E. Maeda, H.D. Shin, Y.M. Cho, K.S. Park, H.K. Lee, M.C. Ng, R.C. Ma, W.Y. So, J.C. Chan, V. Lyssenko, T. Tuomi, P. Nilsson, L. Groop, N. Kamatani, A. Sekine, Y. Nakamura, K. Yamamoto, T. Yoshida, K. Tokunaga, M. Itakura, H. Makino, K. Nanjo, T. Kadowaki, M. Kasuga, Variants in KCNQ1 are associated with susceptibility to type 2 diabetes mellitus, Nat. Genet. 40 (2008) 1092–1097.
[7] H. Unoki, A. Takahashi, T. Kawaguchi, K. Hara, M. Horikoshi, G. Andersen, D.P. Ng, J. Holmkvist, K. Borch-Johnsen, T. Jrgensen, A. Sandbaek, T. Lauritzen, T. Hansen, S. Nurbaya, T. Tsunoda, M. Kubo, T. Babazono, H. Hirose, M. Hayashi, Y. Iwamoto, A. Kashiwagi, K. Kaku, R. Kawamori, E.S. Tai, O. Pedersen, N. Kamatani, T. Kadowaki, R. Kikkawa, Y. Nakamura, S. Maeda, SNPs in KCNQ1 are associated with susceptibility to type 2 diabetes in East Asian and European populations, Nat. Genet. 40 (2008) 1098–1102.
[8] K. Müssig, H. Staiger, F. Machicao, K. Kirchhoff, M. Guthoff, S.A. Schäfer, K. Kantartzis, G. Silbernagel, N. Stefan, J.J. Holst, B. Gallwitz, H.U. Häring, A. Fritsche, Association of type 2 diabetes candidate polymorphisms in KCNQ1 with incretin and insulin secretion, Diabetes 58 (2009) 1715–1720.
[9] J.T. Tan, S. Nurbaya, D. Gardner, S. Ye, E.S. Tai, D.P. Ng, Genetic variation in KCNQ1 associates with fasting glucose and beta-cell function: a study of 3,734 subjects comprising three ethnicities living in Singapore, Diabetes 58 (2009) 1445–1449.
[10] S. Ullrich, J. Su, F. Ranta, O.H. Wittekindt, F. Ris, M. Rösler, U. Gerlach, D. Heitzmann, R. Warth, F. Lang, Effects of I_{Ks} channel inhibitors in insulin-secreting INS-1 cells, Pflugers Arch. 451 (2005) 428–436.
[11] J. Miyazaki, K. Araki, E. Yamato, H. Ikegami, T. Asano, Y. Shibasaki, Y. Oka, K. Yamamura, Establishment of a pancreatic beta cell line that retains glucose-inducible insulin secretion: special reference to expression of glucose transporter isoforms, Endocrinology 127 (1990) 126–132.
[12] S. Morita, T. Kojima, T. Kitamura, Plat-E: an efficient and stable system for transient packaging of retroviruses, Gene Ther. 7 (2000) 1063–1066.
[13] K. Yamagata, T. Nammo, M. Moriwaki, A. Ihara, K. Iizuka, Q. Yang, T. Satoh, M. Li, R. Uenaka, K. Okita, H. Iwahashi, Q. Zhu, Y. Cao, A. Imagawa, Y. Tochino, T. Hanafusa, J. Miyagawa, Y. Matsuzawa, Overexpression of dominant-negative mutant hepatocyte nuclear fctor-1 alpha in pancreatic beta-cells causes abnormal islet architecture with decreased expression of E-cadherin, reduced beta-cell proliferation, and diabetes, Diabetes 51 (2002) 114–123.
[14] T. Kitamura, Y. Koshino, F. Shibata, T. Oki, H. Nakajima, T. Nosaka, H. Kumagai, Retrovirus-mediated gene transfer and expression cloning: powerful tools in functional genomics, Exp. Hematol. 31 (2003) 1007–1014.
[15] Y. Sato, H. Endo, H. Okuyama, T. Takeda, H. Iwahashi, A. Imagawa, K. Yamagata, I. Shimomura, M. Inoue, Cellular hypoxia of pancreatic β-cells due to high levels of oxygen consumption for insulin secretion in vitro. J. Biol. Chem. (2011), doi:10.1074/jbc.M110.194738 [Epub ahead of print]. PMD:21296882.
[16] K. Yamagata, Q. Yang, K. Yamamoto, H. Iwahashi, J. Miyagawa, K. Okita, I. Yoshiuchi, J. Miyazaki, T. Noguchi, H. Nakajima, M. Namba, T. Hanafusa, Y. Matsuzawa, Mutation P291fsinsC in the transcription factor hepatocyte nuclear factor-1α is dominant negative, Diabetes 47 (1998) 1231–1235.
[17] S. Hattori, F. Murakami, W.J. Song, Quantitative relationship between Kv4.2 mRNA and A-type potassium current in rat striatal cholinergic interneurons during postnatal development, J. Neurophysiol. 90 (2003) 175–183.
[18] A. Miura, K. Yamagata, M. Kakei, H. Hatakeyama, N. Takahashi, K. Fukui, T. Nammo, K. Yoneda, Y. Inoue, F.M. Sladek, M.A. Magnuson, H. Kasai, J. Miyagawa, F.J. Gonzalez, I. Shimomura, Hepatocyte nuclear factor-4α is essential for glucose-stimulated insulin secretion by pancreatic β-cells, J. Biol. Chem. 281 (2006) 5246–5257.
[19] D. Peroz, S. Dahimène, I. Baró, G. Loussouarn, J. Mérot, LQT1-associated mutations increase KCNQ1 proteasomal degradation independently of Derlin-1, J. Biol. Chem. 284 (2009) 5250–5256.
[20] W.J. Song, Y. Baba, T. Otsuka, F. Murakami, Characterization of Ca2+ channels in rat subthalamic nucleus neurons, J. Neurophysiol. 84 (2000) 2630–2637.
[21] P.E. MacDonald, M.B. Wheeler, Voltage-dependent K^+ channels in pancreatic beta cells: role, regulation and potential as therapeutic targets, Diabetologia 46 (2003) 1046–1062.
[22] W.S. Zawalich, R. Rognstad, A.S. Pagliara, F.M. Matschinsky, A comparison of the utilization rates and hormone-releasing actions of glucose, mannose, and fructose in isolated pancreatic islets, J. Biol. Chem. 252 (1977) 8519–8523.
[23] J.J. Holst, T. Vilsbll, C.F. Deacon, The incretin system and its role in type 2 diabetes, Mol. Cell Endocrinol. 287 (2009) 127–136.
[24] K.M. Boini, D. Graf, A.M. Hennige, S. Koka, D.S. Kempe, K. Wang, T.F. Ackermann, M. Föller, V. Vallon, K. Pfeifer, E. Schleicher, S. Ullrich, H.U. Häring, D. Häussinger, F. Lang, Enhanced insulin sensitivity of gene-targeted mice lacking functional KCNQ1, Am. J. Physiol. Regul. Integr. Comp. Physiol. 296 (2009) R1695–1701.
[25] K. Nakajo, M.H. Ulbrich, Y. Kubo, E.Y. Isacoff, Stoichiometry of the KCNQ1–KCNE1 ion channel complex, Proc. Natl. Acad. Sci. USA 107 (2010) 18862–18867.
[26] P.E. MacDonald, A.M. Salapatek, M.B. Wheeler, Glucagon-like peptide-1 receptor activation antagonizes voltage-dependent repolarizing K^+ currents in β-cells: a possible glucose-dependent insulinotropic mechanism, Diabetes 51 (2002) S443–447.

THE JOURNAL OF BIOLOGICAL CHEMISTRY VOL. 286, NO. 5, pp. 3992–4002, February 4, 2011

Mitochondrial Dysfunction and Increased Reactive Oxygen Species Impair Insulin Secretion in Sphingomyelin Synthase 1-null Mice*[S]

Received for publication, August 26, 2010, and in revised form, November 8, 2010 Published, JBC Papers in Press, November 29, 2010, DOI 10.1074/jbc.M110.179176

Masato Yano[‡1], Ken Watanabe[§], Tadashi Yamamoto[‡¶], Kazutaka Ikeda[‖], Takafumi Senokuchi[**], Meihong Lu[‡‡], Tsuyoshi Kadomatsu[‡], Hiroto Tsukano[‡], Masahito Ikawa[§§], Masaru Okabe[§§], Shohei Yamaoka[¶¶], Toshiro Okazaki[¶¶], Hisanori Umehara[‖‖], Tomomi Gotoh[‡], Wen-Jie Song[‡‡], Koichi Node[¶], Ryo Taguchi[‖], Kazuya Yamagata[**], and Yuichi Oike[‡2]

From the Departments of [‡]Molecular Genetics, [**]Medical Biochemistry, and [‡‡]Sensory and Cognitive Physiology, Faculty of Life Sciences, Kumamoto University, Kumamoto 860-8556, Japan, the [§]Department of Bone & Joint Disease, National Center for Geriatrics & Gerontology, Aichi 474-8511, Japan, the [¶]Department of Cardiovascular and Renal Medicine, Saga University, Saga 849-8501, Japan, the [‖]Department of Metabolome, Graduate School of Medicine, University of Tokyo, Tokyo 113-0033, Japan, the [§§]Research Institute for Microbial Diseases and Pharmaceutical Sciences, Osaka University, Osaka 565-0871, Japan, the [¶¶]Division of Clinical Laboratory Medicine and Hematology/Oncology, Faculty of Medicine, Tottori University, Tottori 683-8503, Japan, and the [‖‖]Department of Hematology and Immunology, Kanazawa Medical University, Ishikawa 920-0293, Japan

Sphingomyelin synthase 1 (SMS1) catalyzes the conversion of ceramide to sphingomyelin. Here, we generated and analyzed SMS1-null mice. SMS1-null mice exhibited moderate neonatal lethality, reduced body weight, and loss of fat tissues mass, suggesting that they might have metabolic abnormality. Indeed, analysis on glucose metabolism revealed that they showed severe deficiencies in insulin secretion. Isolated mutant islets exhibited severely impaired ability to release insulin, dependent on glucose stimuli. Further analysis indicated that mitochondria in mutant islet cells cannot up-regulate ATP production in response to glucose. We also observed additional mitochondrial abnormalities, such as hyperpolarized membrane potential and increased levels of reactive oxygen species (ROS) in mutant islets. Finally, when SMS1-null mice were treated with the anti-oxidant *N*-acetyl cysteine, we observed partial recovery of insulin secretion, indicating that ROS overproduction underlies pancreatic β-cell dysfunction in SMS1-null mice. Altogether, our data suggest that SMS1 is important for controlling ROS generation, and that SMS1 is required for normal mitochondrial function and insulin secretion in pancreatic β-cells.

Sphingolipids are important for stabilizing membrane structure (1, 2), cell-to-cell recognition, and signaling (3, 4). Some intermediates of sphingolipid metabolism function as second messengers in angiogenesis, cell growth, differentiation, and apoptosis (5–7). One intermediate, ceramide, is a key metabolite in both anabolic and catabolic pathways of sphingolipids (8), and it reportedly mediates cell differentiation, stress responses, and apoptosis (2). The function of ceramide in apoptosis is clinically significant, because many cancer chemotherapies apparently induce ceramide-dependent apoptosis (9–11). Although perturbance of ceramide homeostasis is related to many diseases, the function of ceramide in these conditions remains uncharacterized.

Sphingolipids are synthesized vectorially in cells. The initial step involves condensation of serine and a fatty acyl-Co-A, generating ceramide in the endoplasmic reticulum (ER),[3] followed by a series of reactions (supplemental Fig. S1) (12, 13). Newly synthesized ceramide is then transported from the ER to the Golgi complex by ceramide transfer protein, CERT (14, 15). Ceramide is converted to sphingomyelin by sphingomyelin synthase 1 (SMS1) in the Golgi complex (13, 16). Sphingomyelin is then transferred to the plasma membrane by exocytic vesicles and reversibly converted into ceramide by sphingomyelin synthase 2 (SMS2) on the plasma membrane.

Recently, several investigators have used mutant mice to analyze ceramide trafficking. CERT mutant mice exhibit embryonic lethality attributable to mitochondrial degeneration (17). CERT importance has also been demonstrated in *Drosophila melanogaster*, in which CERT-null flies exhibit a higher oxidative stress response and a shortened lifespan (18). SMS2 mutant mice exhibit an attenuated inflammatory response in macrophages (19) and reduced sphingomyelin levels in plasma and liver (20). However, the effect of SMS1 ablation *in vivo* has not been examined, although it has been analyzed in cultured cells in which investigators found that SMS1 plays a critical role in proliferation of mouse lymphoid cells (16). Membrane sphingomyelin is reportedly important for Fas clustering through aggregation of lipid rafts, leading to

* This work was supported by Grants-in-Aid 19790215 (to M. Y.), and 22116009 (to Y. O.) from the Ministry of Education, Science, Technology, Sports, and Culture of Japan, by Grant-in-Aid 22659156 (to Y. O.) from the Japan Society for the Promotion of Science, and by grants-in-aid from the Takeda Science Foundation and Inamori Foundation (to M. Y.).

[S] The on-line version of this article (available at http://www.jbc.org) contains supplemental Figs. S1 and S2 and Table S1.

[1] To whom correspondence may be addressed. Tel.: 81-96-373-5143; Fax: 81-96-373-5145; E-mail: myano@gpo.kumamoto-u.ac.jp.

[2] To whom correspondence may be addressed. Tel.: 81-96-373-5143; Fax: 81-96-373-5145; E-mail: oike@gpo.kumamoto-u.ac.jp.

[3] The abbreviations used are: ER, endoplasmic reticulum; CERT, ceramide transfer protein; SMS1, sphingomyelin synthase 1; ROS, reactive oxygen species; GTT, glucose tolerance test; ITT, insulin tolerance test; NAC, *N*-acetyl cysteine; KO, knock-out; WAT, white adipose tissue.

Fas-mediated apoptosis (21). Suppression of SMS1 also results in enhanced ceramide production and apoptosis after photodamage (22).

Here, we generated SMS1 knock-out (SMS1-KO) mice. They exhibited moderate neonatal lethality, reduced body weight, and loss of fat tissues mass, suggesting that they might have metabolic abnormality. Then, we first analyzed glucose metabolism of the mice, and found that SMS1-KO mice showed severe deficiencies in insulin secretion. Therefore, in this study, we focused on the analysis to reveal the reason why insulin secretion was reduced in SMS1-KO mice. Isolated SMS1-KO islets exhibited severe deficiency in insulin release dependent on glucose stimuli. SMS1-KO islet mitochondria showed abnormalities, such as decreased ATP production, hyperpolarized membrane potential, and increased ROS. These results suggest that increased ROS production followed by mitochondrial dysfunction impairs insulin secretion in SMS1-KO mice. Strikingly, insulin release deficiency was rescued when SMS1-KO mice were supplied an anti-oxidant reagent, suggesting that ROS over-production underlies mitochondrial dysfunction of SMS1-KO pancreatic β-cells. Altogether, our data suggest that SMS1 is important for controlling ROS generation, and that SMS1 is required for normal mitochondrial function and normal insulin secretion in pancreatic β-cells.

EXPERIMENTAL PROCEDURES

Materials and Reagents—All reagents were supplied by Sigma-Aldrich or Wako (Osaka, Japan), unless otherwise stated. Urinary 8-hydroxydeoxy-guanosine (8-OHdG) levels were measured using an ELISA kit (Nikken Seil, Shizuoka, Japan). *N*-[7-(4-nitrobenzo-2-oxa-1,3-diazole)]-6-aminocaproyl-D-erythro-sphingosine (C_6-NBD-ceramide) was purchased from Cayman Chemical (Ann Arbor, MI).

Generation of SMS1-KO Mice—Genomic DNA clones of the *Sms1* locus were isolated from a mouse 129/Svj genomic library (Stratagene, Santa Clara, CA) using full-length Sms1 cDNA as a probe. Exon 2, which encodes the translation initiation codon, the SAM domain and two SMS1 transmembrane regions, was replaced with a neo cassette. An 8-kbp EcoRI fragment containing the intron between exons 2 and 3 as a long arm and a 1 kbp EcoRI/PstI fragment of regions upstream of exon 2 as a short arm were inserted into pPGKneo(wt). The gene encoding the diphtheria toxin A fragment (DT-A) from pMC1-DT-A was inserted into the end of the long arm as a negative selection marker. The targeting vector was linearized, electroporated into D3 embryonic stem (ES) cells, and clones were selected in G418. Targeting events were screened by PCR and confirmed by Southern blot analysis. Recombinant cells were karyotyped to ensure that 2N chromosomes were present in most metaphase spreads. Chimeric mice derived from correctly targeted ES cells were mated with C57BL/6 mice to obtain F1 *Sms1*$^{+/-}$ mice. All experiments were performed using F3 generation mice. PCR primers used to distinguish targeted from wild-type alleles were: GOR2SAp3, 5′-TTTGAGGAGAGAGGCCTTGAGTCTC-3′; GOR2-R1, 5′-AGGCAGCCACTTCCAGCAGCCAG-3′; and PGKneoS, 5′-TCGCCTTCTATCGCCTTCTTGAC-3′. GOR2SAp3 and GOR2-R1 primers amplified a 381 bp DNA fragment from the wild-type allele, whereas GOR2SAp3 and PGKneoS primers amplified a 552-bp fragment from the targeted allele. PCR was carried out with 30 cycles consisting of 94.5 °C, 1 min; 60 °C, 1 min; 72 °C, 1 min.

Long and Accurate (LA)-PCR—To confirm the homologous recombination, PCR was performed. For detection short arm, KOD-Fx (TOYOBO, Osaka, Japan) was used according to the manufacturer's protocol. The primer sequences are as follows; (a) GOR2-SA1, 5′-GGGCTATCAGAAACTTCTTGATG-3′, (b) GOR2-R1, 5′-AGGCAGCCACTTCCAGCAGCCAG-3′, (c) PGKneoS, 5′-TCGCCTTCTATCGCCTTCTTGAC-3′. Long-accurate (LA)-PCR was performed for confirm the recombination in long arm. The protocol for the LA-PCR is as follows; an initial denature step, 95 °C, 1 min; 30 cycles of 98 °C, 10 s and 68 °C, 15 min, using LA-Taq (TAKARA, Kyoto, Japan). The primers used are as follows; (d) GOR2WT-LA-2F, 5′-GAGTGGTTTCCTGGTGTTGGATAAAGTC-3′, (e) NML1, 5′-GCCTACCCGCTTCCATTGCTCAGC-3′, (f) GOR2-FLA-2R, 5′-CCTGTTTAGAGCTTCGTCTCTTACTC-3′.

Northern Blotting—Total RNA was isolated from embryonic fibroblasts using RNeasy kit (Qiagen, Valencia, CA). Ten micrograms of total RNA were electrophoresed and blotted onto nylon membrane. The hybridization was performed using full-length (FL) or a PCR fragment (ex2) corresponding to SAM domain of mouse SMS1 cDNA as a ^{32}P-labeled probe. The washed membranes were exposed to imaging plates, and the signals were developed by BAS2000 system (Fujifilm, Tokyo, Japan).

TLC Analysis of Sphingomyelin Synthase (SMS) and Glycosylceramide Synthase (GCS) Activity—Genes for wild-type SMS1 and mutant SMS1 (SMS1 Δex2), in which exon 2 region encoding the translation initiation codon, the SAM domain and two SMS1 transmembrane regions was deleted, were transducted in WR19L/Fas-SM(−) cells by retro virus system (16). The cells were homogenized in an ice-cold buffer containing 20 mM Tris-HCl, pH 7.4, 2 mM EDTA, 10 mM EGTA, 1 mM phenylmethylsulfonyl fluoride, and 2.5 μg/ml leupeptin. The lysates containing 100 μg of cell protein were added to a reaction solution containing 10 mM Tris-HCl, pH 7.5, 1 mM EDTA, 20 μM C_6-NBD-ceramide, 120 μM phosphatidylcholine (PC), and incubated at 37 °C for 60 min. The lipids were extracted by the method of Bligh and Dyer (23), applied on the thin-layer chromatgraphy (TLC) plates, and developed with solvent containing chloroform/methanol/12 mM $MgCl_2$ in H_2O (65:25:4). The fluorescent lipids were visualized by LAS-1000 system (Fujifilm).

Animal Studies—Animals were housed in a temperature-controlled room with a 12-h light/dark cycle. Food and water were available *ad libitum* unless noted. Mice were fed a normal diet (CE-2; CLEA, Japan). NAC (40 mM) was administered in drinking water. All experimental protocols were approved by the Ethics Review Committee for Animal Experimentation of Kumamoto University.

Metabolic Measurements—Glucose tolerance test (GTT) and insulin tolerance test (ITT) were performed as described (24). For GTT, mice were deprived of food for 16 h and injected intraperitoneally with 1 mg/kg glucose. For ITT, mice

were administered 1 unit/kg of human insulin by intraperitoneal injection. Blood was withdrawn from the supraorbital plexus at times indicated in figures. Blood glucose was measured using the glucose oxidase method (Sanwa Kagaku, Nagoya, Japan), and serum insulin was measured by using an ELISA kit (Morinaga Institute of Biological Science, Yokohama, Japan).

Morphological Analysis of Pancreatic Islets—Pancreas tissues isolated from wild-type or mutant mice were fixed in 4% paraformaldehyde, and random sections were generated. Islet number per unit area of pancreas and islet size were measured using hematoxylin-eosin-stained sections. For immunohistochemistry, sections were incubated with anti-insulin guinea pig IgG (Affinity BioReagents, Rockford, IL) and anti-glucagon rabbit polyclonal antibody (Thermo Scientific, Waltham, MA) at 1:200 dilutions. Samples were then incubated in Alexa Fluor 647-labeled goat anti-guinea pig IgG and Alexa Fluor 488-labeled goat anti-rabbit IgG (Molecular Probes, Eugene, OR). Immunofluorescence for insulin and glucagon was observed using a Biorevo BZ-9000 fluorescence microscope (Keyence, Osaka, Japan).

Isolation of Pancreatic Islets—Mouse pancreatic islets were isolated by collagenase digestion as described (25, 26) with slight modification. Mice were anesthetized by intraperitoneal injection of thiopental sodium. Collagenase (collagenase type S-1, 0.6 mg/ml; Nitta Gelatin, Osaka, Japan) was dissolved in Hanks' Balanced Salt Solutions (Sigma) with 800 KI units/ml aprotinin (Wako). Collagenase solution was injected into the common bile duct. Pancreata were dissected and incubated in collagenase solution at 37 °C for 20 min with shaking. The solution was then mixed with ice-cold isotonic sucrose buffer and chilled on ice for 20 min. Precipitated islets were collected for further experiments.

Quantitative RT-PCR—Total RNA from islet tissues was isolated with TRIzol reagent (Invitrogen), and DNase-treated RNA was reverse transcribed with a PrimeScript RT reagent kit (Takara Bio, Osaka, Japan), following the manufacturer's protocol. PCR products were analyzed using a Thermal Cycler Dice Real Time system (Takara Bio), and transcript abundance was normalized to that of β-actin mRNA. PCR oligonucleotides and gene abbreviations are listed in supplemental Table S1.

Measurement of Insulin Release from Islets—Groups of 10–15 islets were incubated for 1 h in Ca^{2+}-containing HEPES-added Krebs-Ringer bicarbonate buffer (HKRB) solution (129 mM NaCl, 1.2 mM $MgSO_4$, 1.2 mM KH_2PO_4, 4.7 mM KCl, 5 mM $NaHCO_3$, 2.5 mM $CaCl_2$, 10 mM HEPES, pH7.4, with 0.05% bovine serum albumin) with 2.2 mM glucose at 37 °C under 5% CO_2 atmosphere stabilization, followed by test incubation for 1 h in HKRB with 2.2 or 22 mM glucose. The concentration of secreted insulin was determined by using an ELISA kit (Medical & Biological Laboratories).

Measurement of ATP Levels, Mitochondrial Membrane Potential, and ROS Production—To measure ATP content in islet cells, groups of 20–30 islets were incubated for 1 h in HKRB with 2.2 mM or 22 mM glucose at 37 °C. ATP in islets was extracted in 0.1% trichloroacetic acid and neutralized in 0.1 M Tris acetate. ATP levels were measured using a Cellular ATP Assay Kit (Toyo Ink, Tokyo, Japan) using Luminometer Model TD-20/20 (Promega, San Luis Obispo, CA). To measure mitochondrial membrane potential, groups of 20–30 islets were loaded with JC-1 (Invitrogen, Carlsbad, CA) by incubation in HKRB with 2.2 or 22 mM glucose at 37 °C for 1 h. Red and green fluorescence was observed under a fluorescence microscope. Red fluorescence was also monitored in a plate-reader fluorometer, Fluoroskan Ascent (Thermo Labsystem, Helsinki, Finland). To measure ROS production in islets, groups of 20–30 islets were incubated in HKRB with 2.2 mM glucose in the presence of CM-H_2DCFDA (Invitrogen). Green fluorescence derived from ROS generation was monitored in a plate-reader fluorometer.

Isolation of Pancreatic Mitochondria—Mitochondria were isolated as described (27, 28) with minor modifications. Pancreas tissues were isolated and minced in mitochondria isolation buffer (3 mM HEPES-KOH, pH 7.5, 210 mM mannitol, 70 mM sucrose, 0.2 mM EGTA) containing a protease inhibitor mixture (Roche, Basel, Switzerland). Samples were disrupted using a tissue grinder (Iwaki, Tokyo, Japan), and homogenates were centrifuged at 500 × *g* for 5 min to remove nuclei and unbroken cells followed by centrifugation at 10,000 × *g* for 5 min to obtain the mitochondrial pellet. The pellet was suspended in mitochondria isolation buffer and purified by consecutive centrifugations (500 × *g* for 5 min twice to recover the supernatant and at 10,000 × *g* three times to recover the pellet). All procedures were performed under ice-cold conditions.

Sphingolipid Extraction and LC/ESI-MS Analysis—Total lipids from islets or pancreas mitochondria from wild-type and SMS1-KO mice were extracted with 1 ml methanol for 1 h at room temperature. In this process, 1 nmol of sphingomyelin (d18:1/12:0) and ceramide (d18:1/12:0) were added as internal standards. Extracts were centrifuged at 10000 × *g* for 15 min, and the supernatant was collected and re-dissolved with chloroform:methanol (2:1; v/v) after drying under a gentle nitrogen stream. LC/ESI-MS analysis was performed using a quadrapole/time of flight hybrid mass spectrometer (Q-TOF micro) with an ACQUITY UPLC system (Waters Corp., Milford, MA). The scan range was set at *m/z* 200–1100 and scan duration of MS and MS/MS at 0.5 s in negative ion mode (29, 30). The capillary voltage was set at 2.5 kV, cone voltage at −30 V and collision energy for MS/MS analysis at −30 V. Reverse-phased LC separation was achieved using an ACQUITY UPLC BEH C18 column (1.0 × 150 mm i.d., Waters Corporation) at 45 °C. 2 μl of total lipids normalized to protein content were individually injected. The mobile phase was acetonitrile/methanol/water (19/19/2) (0.1% formic acid + 0.028% ammonia) (*A*), and isopropanol (0.1% formic acid + 0.028% ammonia) (*B*), and the composition was produced by mixing these solvents. The gradient consisted of holding in (A/B: 90/10) solvent for 7.5 min, and then linearly converting to solvent (A/B: 70/30) for 32.5 min and finally converting to solvent (A/B: 40/60) for 50 min. The mobile phase was pumped at a flow rate of 40–50 μl/min. MS data processing was applied using Mass++ software to detect each chromatogram peak with quantitative accuracy.

Immunoblot Analysis—Isolated islets were solubilized in PBS containing 1% SDS. Total protein was separated by SDS-PAGE, transferred to nitrocellulose membranes, and analyzed with ECL Western blotting Detection Reagents (GE Healthcare, Buckinghamshire, England). Immunoblotting was performed with anti-Hsc70 antibody (Santa Cruz Biotechnology, Santa Cruz, CA), anti-4-hydroxy-2-nonenal (4-HNE) antibody (R&D Systems, Minneapolis, MN), anti-Complex I NDUFA9 (αs9) antibody (Invitrogen), anti-Complex II 70 kDa subunit (Fp) antibody (Invitrogen), or anti-Complex III subunit core 2 (QCR2) antibody (Invitrogen).

Statistical Analysis—Data were analyzed using Student's *t* test and reported as means ± S.E., unless stated. Indicated significance levels are: *, $p < 0.05$; **, $p < 0.01$; ***, $p < 0.001$.

RESULTS

Targeted Disruption of SMS1 Gene Eliminate SMS1 Activity—To analyze the effect of SMS1 ablation *in vivo*, we generated SMS1-null (SMS1-KO) mice (Fig. 1). Exon 2 of *SMS1* gene, which encodes the translation initiation codon, the SAM domain and two transmembrane regions, was replaced with a neo cassette (Fig. 1*A*). The allele, designated SMS1-KO, was established and confirmed by LA-PCR (Fig. 1*B*). Deletion of the region corresponding to exon 2 in SMS1 mRNA derived from SMS1-KO mice was confirmed by northern-blot analysis (Fig. 1*C*). To confirm that this SMS1-KO construct, which may express N-terminal deletion mutant of SMS1 (SMS1Δex2), does not exhibit sphingomyelin synthase (SMS) activity, we measured SMS activity of SMS1Δex2 in SMS activity null cells (Fig. 1*D*). Although wild-type SMS1 produce a significant amount of sphingomyelin (SM) derivative (NDB-SM), SMS1Δex2 did not, suggesting that SMS1Δex2 has no SMS activity. Thus, we concluded that the activity of SMS1 was completely disrupted in SMS1-KO mice used in this study. Conventionally, we used PCR technique to distinguish wild-type, heterozygous, and KO mice (Fig. 1*E*).

SMS1-KO Mice Exhibit Reduced Insulin Secretion—We initially observed growth of SMS1-KO mice. They showed moderate neonatal lethality with half of mice dead by 10 weeks (Fig. 2*A*), suggesting that SMS1 gene is important for normal growth of mice. And, we found that the body weight of SMS1-KO mice was reduced (Fig. 2*B*). To investigate the reason, we anatomically analyzed and found that the mass of white adipose tissue (WAT) was significantly reduced (Fig. 2*C*). These results suggested that SMS1-KO mice might have metabolic deficiency.

Then, we next examined the possibility whether blood glucose homeostasis was affected by SMS1 ablation. Blood tests indicated that SMS1-KO mice exhibited hyperglycemia after 16 h of fasting, suggesting impaired glucose homeostasis (Fig. 2*D*). Glucose tolerance tests (GTT) further indicated that glucose uptake of SMS1-KO mice was impaired (Fig. 2*E*). Analysis of insulin in serum samples obtained from GTTs showed that glucose-induced insulin release was significantly reduced in SMS1-KO mice (Fig. 2*F*). However, SMS1-KO mice exhibited higher insulin sensitivity compared with wild-type mice based on insulin tolerance tests (ITT) (Fig. 2*G*). Therefore, we concluded that lower glucose uptake seen in SMS1-KO mice was due to impaired insulin secretion. In the following experiments, we focused on the analysis to reveal the reason why insulin secretion was reduced in SMS1-KO mice.

Pancreatic β-cell Death Does Not Underlie Insulin Secretion Deficiencies Seen in SMS1-KO Mice—Because SMS1 ablation will enhance accumulation of ceramide, an enzymatic substrate of SMS1, we first measured the amount of sphingolipid species in SMS1-KO islets by LC/ESI-MS analysis (Fig. 3, *A–C*). As expected, the amount of sphingomyelin species was reduced (Fig. 3*A*), whereas the amount of ceramide species was increased in SMS1-KO islets (Fig. 3*B*). The amount of phosphatidylcholine, another substrate of SMS1, seemed to be a little increased (about 1.2-fold), but the increment was not significant (data not shown). The amount of GM3, a glycosphingolipid, was also increased (Fig. 3*C*), suggesting that accumulated ceramide species were alternatively metabolized into glycosphingolipid species. However, we could not find any significant change of expression of mRNAs for sphingolipid metabolisms (Fig. 3*D* and supplemental Fig. S1 and Table S1).

Because ceramide reportedly promotes cell death (31, 32), we estimated that loss of insulin secretion in SMS1-KO mice might be attributable to ceramide-induced death of pancreatic β-cells. To test this possibility, we examined expression of mRNAs related to apoptosis. However, no significant changes were observed in expression of apoptosis-inducing factors (Bax and CHOP) or apoptosis-inhibiting factors (Bip, Bcl-2, Bcl-X and Mcl-1) (Fig. 3*E* and supplemental Table S1). In addition, we observed no difference in islet size (Fig. 3*F*), density (Fig. 3*G*), or morphology (Fig. 3, *H* and *I*). These results suggest that pancreatic β-cell death does not underlie the insulin secretion deficiency seen in SMS1-KO mice.

SMS1-KO Islets Exhibit Decreased Insulin Secretion Accompanied by Mitochondrial Abnormalities—To determine the primary cause of insulin secretion deficiency seen in SMS1-KO mice, we asked whether insulin secretion was reduced in SMS1 deficient islets. First, by an ELISA, we confirmed that the total amount of insulin in isolated SMS1-KO islets was equivalent to that seen in wild-type islets (Fig. 4*A*). When islets were incubated under high glucose (22 mM) conditions, SMS1-KO islets released only low levels of insulin, whereas wild-type islets released large amounts (Fig. 4*B*). Thus, we concluded that insulin secretion deficiency observed in SMS1-KO mice was attributed to insulin secretion deficiency of pancreatic β-cells.

Because SMS1 resides in the Golgi complex, we hypothesized that other intracellular organelles might be damaged by SMS1 deletion. Indeed, intracellular levels of ceramide in ER and mitochondria are reportedly increased when the ceramide transfer protein, CERT, is ablated (17). Then, we focused in particular on the effect of SMS1 loss on mitochondria, because mitochondria are important for insulin secretion (33, 34). Mitochondria were highly purified from pancreas (supplemental Fig. S2). Analysis using LC/ESI-MS revealed that the amounts of some kinds of sphingomyelin species were reduced in pancreatic mitochondria of SMS1-KO mice (Fig. 4*C*), whereas some kinds of ceramide

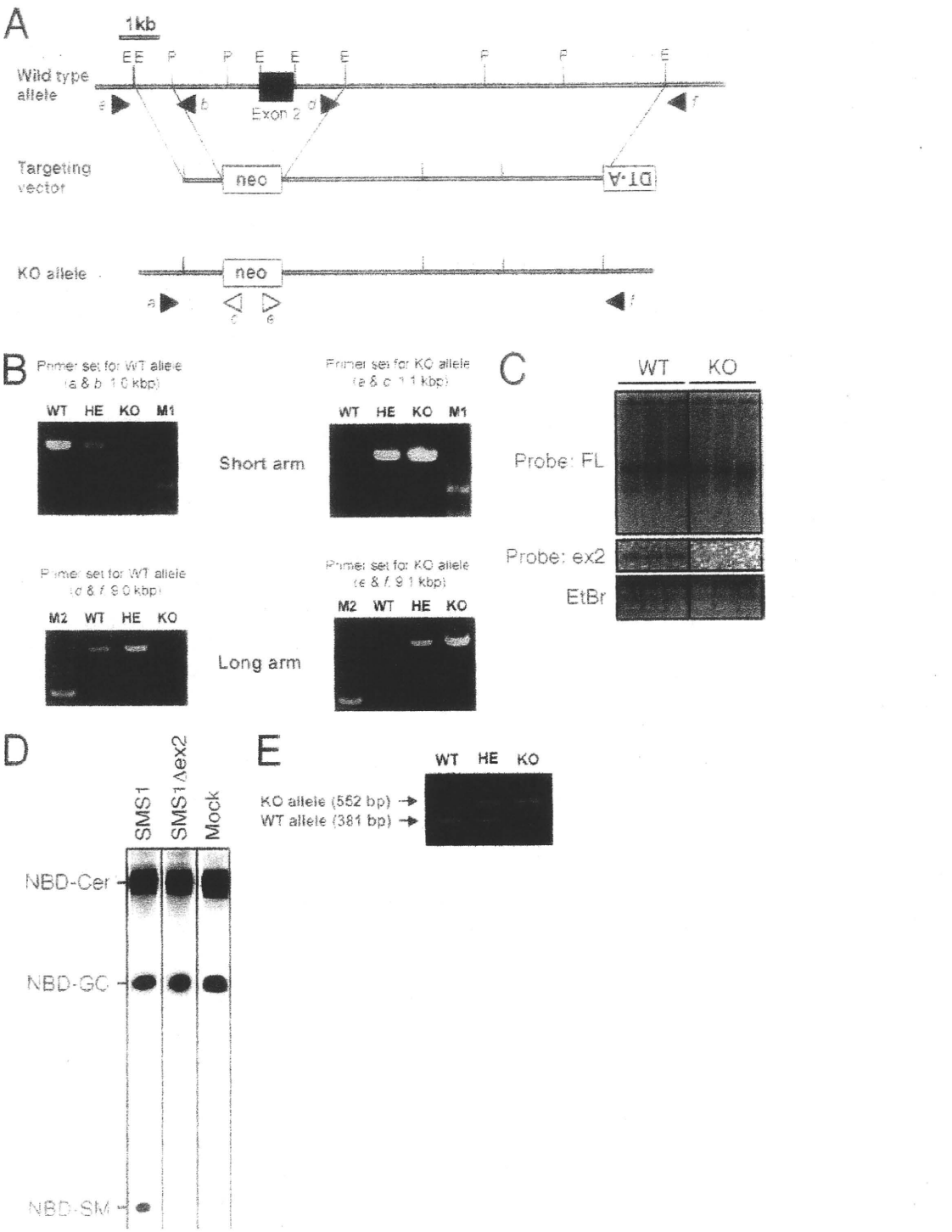

FIGURE 1. **Construction and confirmation of SMS1-KO mice.** *A*, schematic representation of the targeting vector, the wild-type *Sms1* locus, and the mutant allele after homologous recombination. Exon 2 is denoted by *filled boxes*. E and P represent EcoRI and PstI restriction sites, respectively. *Closed* and *open arrowheads* are corresponding to the primer position to detect WT and KO alleles, respectively. Primer sequences are shown in "Experimental Procedures." *B*, confirmation of homologous recombination by PCR. *Upper two panels* show the amplified PCR fragments for WT or KO allele as indicated. A ladder is 100-bp DNA marker (M1). *Lower two panels* show the amplified fragments by LA-PCR. The ladders shown *left* in each panel are of 1-kb DNA ladder (M2). Primer set (*e.g. a* & *b*) for each PCR is shown in *A*. *C*, Northern blot analysis. The results of three each of total RNA was independently isolated from WT or KO. *Top* and *middle panels* showed the hybridized bands detected by full-length cDNA probe (*FL*) and exon 2 probe (*ex2*), respectively. *Bottom panel* showed total RNA stained by ethidium bromide (*EtBr*). *D*, SMS activity of SMS1 and SMS1Δex2. Genes for wild-type SMS1 and mutant SMS1 (SMS1 Δex2), in which exon 2 region encoding the translation initiation codon, the SAM domain and two SMS1 transmembrane regions was deleted in the same manner as SMS1-KO mice, were transducted in SMS activity-null cells by retro virus system. The cell lysates were mixed with C_6-NBD-ceramide and PC and incubated at 37 °C for 60 min. The lipids were extracted and applied on the TLC plates. Mock indicates empty vector. *E*, confirmation of the genotype of newborn mice by PCR. Primer sequences are shown in "Experimental Procedures."

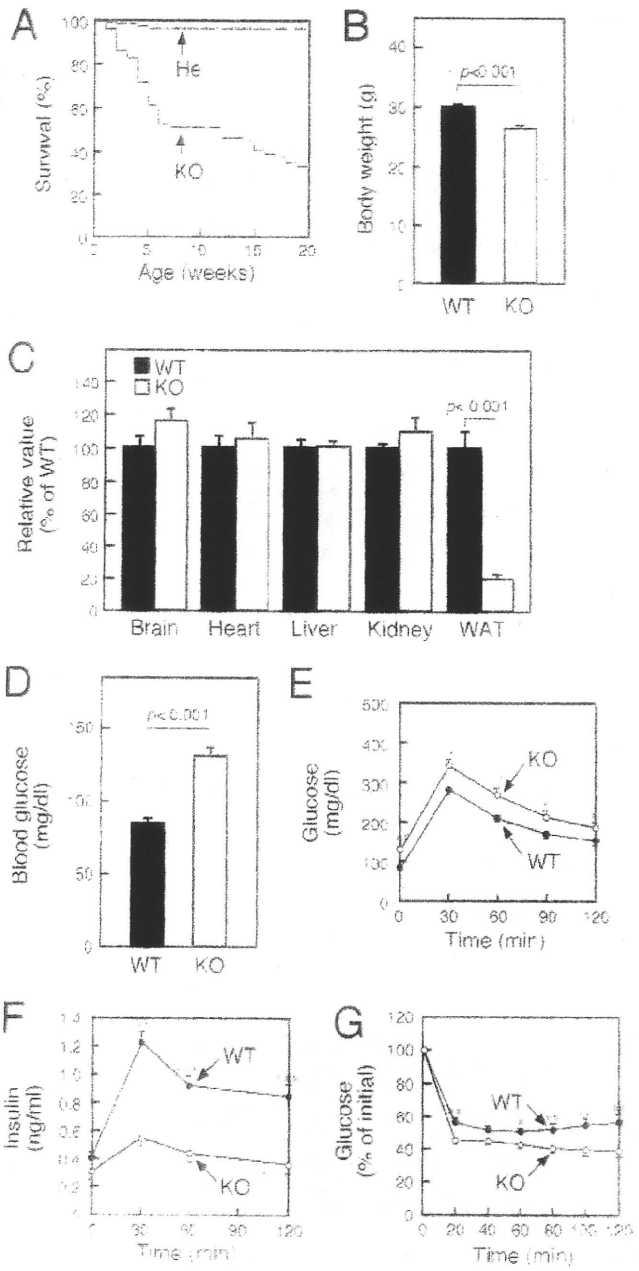

FIGURE 2. **SMS1-KO mice exhibit reduced insulin secretion.** *A*, survival curve of SMS1-KO (*KO*, $n = 68$) and heterozygous (*He*, $n = 153$) mice. *B*, body weights of 10 weeks old wild-type (*WT*, $n = 37$) and SMS1-KO mice (*KO*, $n = 9$). *C*, weight of organs of 10-week-old mice (*WT*, $n = 6$; *KO*, $n = 4$). Mice of 12–16 weeks old were used for the following analysis. *D*, blood glucose levels after 16 h of fasting were measured using the glucose oxidase method (*WT*, $n = 21$; *KO*, $n = 20$). *E*, glucose tolerance tests. Mice were deprived of food for 16 h and injected with 1 mg/kg glucose. Blood was withdrawn at times indicated, and blood glucose was measured (*WT*, $n = 21$; *KO*, $n = 24$). *F*, amounts of insulin in the serum obtained from glucose tolerance tests performed in *E* were measured by an ELISA (*WT*, $n = 32$; *KO*, $n = 25$). *G*, insulin tolerance test. Mice were administered 1 unit/kg of human insulin. Blood was withdrawn at times indicated, and blood glucose was measured (*WT*, $n = 21$; *KO*, $n = 20$). *, $p < 0.05$; **, $p < 0.01$; ***, $p < 0.001$.

species were increased (Fig. 4*D*), suggesting that SMS1-KO mitochondria might exhibit dysfunction.

Because mitochondrial activation and up-regulated ATP synthesis are key steps in insulin secretion (33, 34), we analyzed islet ATP content (Fig. 4*E*). When islets were incubated in low glucose (2.2 mM) condition, no significant difference in ATP content was observed between wild-type and SMS1-KO islets. However, when islets were incubated in high glucose (22 mM) condition, SMS1-KO islets exhibited significantly lower ATP content relative to wild-type islets, indicating that the mitochondria of SMS1-KO pancreatic β-cells have deficiency to synthesize ATP in response to glucose stimulation.

To analyze other mitochondrial anomalies in SMS1-KO pancreatic β-cells, we used the fluorescent dye JC-1 (5′5″6′6′-tetrachloro-1′1″3′3′-tetraethylbenzimidazolylcarbocyanine iodide) to detect mitochondrial membrane potential. JC-1 gives red fluorescence when mitochondrial membrane potential is high, whereas it gives green fluorescence when the potential is low. We found that SMS1-KO islets showed significantly stronger red fluorescence, indicative of increased membrane potential, than did wild-type islets (Fig. 4*F*). Higher mitochondrial membrane potential observed in SMS1-KO islets was seen in both low and high glucose conditions (Fig. 4*G*).

Because SMS1-KO islet exhibited higher mitochondrial membrane potential but lower ATP synthesis, we estimated that the mitochondrial respiratory complex in SMS1-KO pancreatic β-cells cannot transport electrons efficiently, and that breakdown in electron transport may increase ROS production. Indeed, it is reported that increased mitochondrial ceramide directly inhibits mitochondrial respiratory complex III, leading to ROS generation (35–37). Thus, we measured ROS levels in islets using the ROS-reactive fluorescent reagent, 5-(and-6)-chloromethyl-2′,7′-dichlorodihydrofluorescein diacetate, acetyl ester (CM-H_2DCFDA) (Fig. 4*H*). As predicted, ROS levels in SMS1-KO islets were significantly greater than that seen in wild-type cells. Immunoblot analysis of islets and pancreas using anti-4-hydroxy-2-nonenal (4-HNE) antibody, which recognizes ROS-modified proteins, also indicated that ROS levels in SMS1-KO islets and pancreas were significantly greater than that seen in wild-type (Fig. 4*I*). Additionally, 8-hydroxydeoxyguanosine (8-OHdG), a marker of ROS generation, was also increased in the urine of SMS1-KO mice, suggesting that ROS generation increases systemically in SMS1-KO mice (Fig. 4*J*). Because excessive ROS production in mitochondria induce oxidative modification of mitochondrial lipids, proteins, and DNA (38–40), mitochondrial respiration complex components of SMS1-KO islet could be damaged by excessive ROS.

Expression of Mitochondrial Respiratory Complex Components Is Enhanced in SMS1-KO Islets—If mitochondrial proteins, especially mitochondrial respiratory complex components, were damaged by ROS, mRNAs encoding mitochondrial respiratory complex components might be up-regulated to compensate for damage. To examine this possibility, we performed real-time-PCR analysis of islet tissues to assay expression of mRNAs encoding respiratory complex components. These transcripts were up-regulated in SMS1-KO islet cells relative to wild-type cells (Fig. 5*A* and supplemental Table S1). Such increases were particularly significant for mRNAs encoding proteins of Complex I, which is a major source of ROS. Indeed, immunoblot analysis revealed

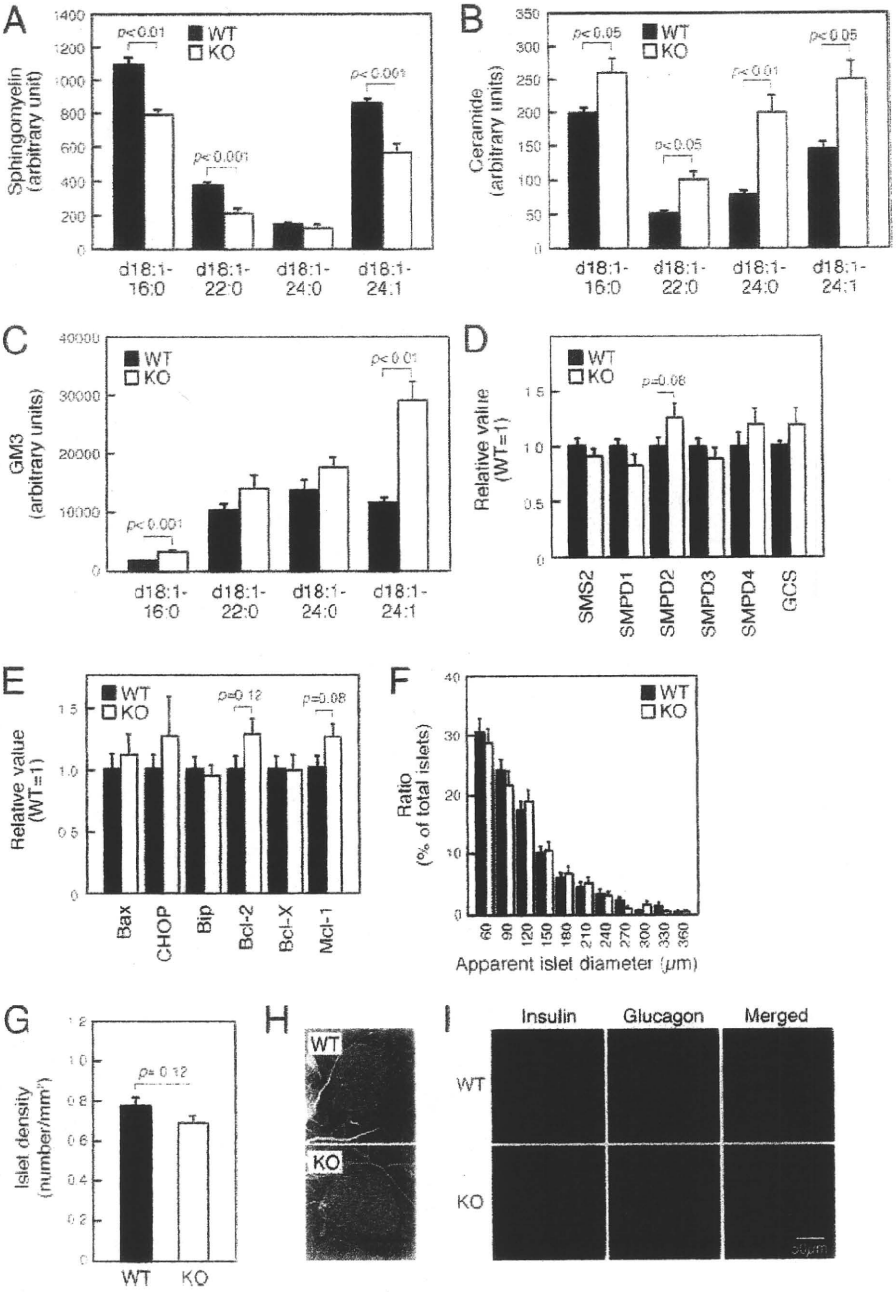

FIGURE 3. **Pancreatic β-cell death is not a cause of insulin secretion deficiency seen in SMS1-KO mice.** Mice, 12–16 of weeks old, were used for analysis. *A–C*, Levels of sphingomyelin (*A*), ceramide (*B*), GM3 (*C*) species in pancreatic islets was measured by LC/ESI-MS. Islets isolated from three mice of the same genotype constituted one sample. $n = 4$ samples per group. *D*, expression levels of genes for sphingolipid metabolism were assessed by quantitative RT-PCR. Islets isolated from two mice of the same genotype served as one sample. Individual measurements were normalized to β-actin expression, and the wild-type group average was set to 1. $n = 6–8$ samples per group. *E*, expression levels of genes encoding factors indicative of apoptosis were assessed by quantitative RT-PCR. $n = 8–12$ samples per group. *F*, apparent diameter of islets seen in cross section (*WT*, $n = 771$; *KO*, $n = 678$). *G*, number of islets per cross-section (*WT*, $n = 102$; *KO*, $n = 104$). *H*, histochemical analysis of islets by hematoxylin-eosin stain. *I*, immunohistochemical analysis of islets for insulin and glucagon.

that protein expression of αs9 (NDUFA9), a component of Complex I, was much higher in SMS1-KO islets (Fig. 5*B*). When expression of mRNAs encoding factors relevant to mitochondrial biogenesis was analyzed, mRNAs for peroxisome proliferator-activated receptor-γ (PPARγ) and PPARγ coactivators (PGC-1α and PGC-1β) were up-regulated in SMS1-KO islets (Fig. 5*C* and Supplemental Table S1), possibly in response to mitochondrial dysfunction induced by ROS. In addition, mitochondrial uncoupling protein 2 (UCP2) was up-regulated in SMS1-KO islets, suggesting a compensatory response to ROS generation at the expense of decreased ATP production (Fig. 5*D* and Supplemental Table S1). Expression of mRNAs encoding ROS detoxification enzymes, such as catalase, was also increased. Overall, these results suggest that major ROS-induced cell responses were enhanced in SMS1-KO islets.

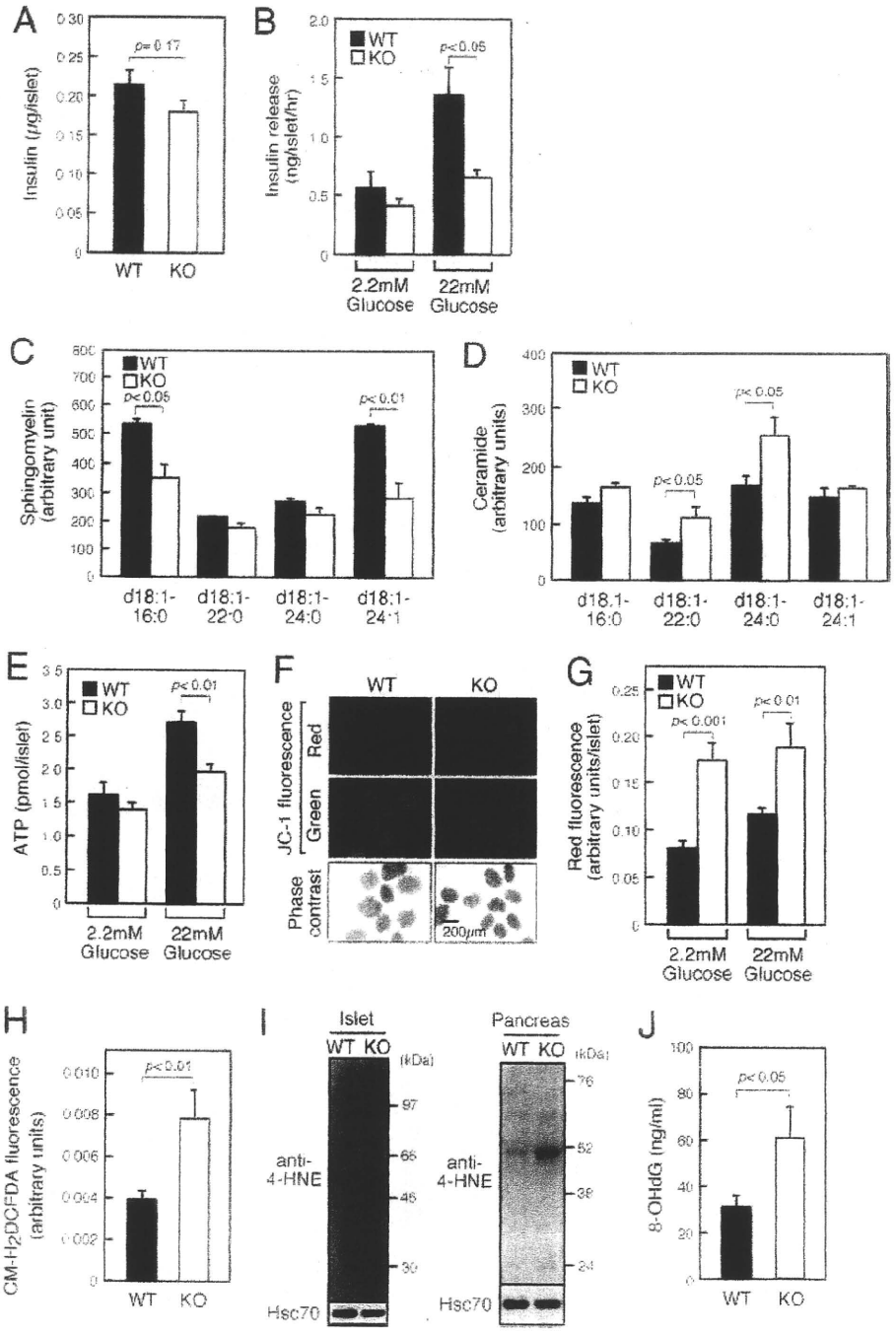

FIGURE 4. **SMS1-KO islets exhibit reduced insulin secretion accompanied by reduced ATP synthesis, increased mitochondrial membrane potential, and increased ROS generation.** Mice of 12–16-week-old were used for analysis. *A*, insulin content in islet protein extracts was examined by an ELISA (*WT*, $n = 10$; *KO*, $n = 6$). *B*, insulin release from isolated islets. Islets were incubated in the presence of 2.2 mM or 22 mM glucose, and released insulin was detected by an ELISA (*WT*, $n = 12$; *KO*, $n = 12$). *C* and *D*, levels of sphingomyelin (*C*) and ceramide (*D*) species in isolated pancreatic mitochondria was analyzed by LC/ESI-MS. $n = 3$ samples per group. *E*, total cellular ATP concentration in isolated islets was determined following a 1-h incubation period in 2.2 mM and 22 mM glucose (*WT*, $n = 16$; *KO*, $n > 15$). *F*, mitochondrial membrane potential was observed by assessing islets loaded with JC-1 following a 1 h-incubation period in 2.2 mM glucose. *G*, quantification of red fluorescence intensity in islets loaded with JC-1 following 1-h incubation in 2.2 mM or 22 mM glucose (*WT*, $n > 19$; *KO*, $n > 17$). *H*, detection of ROS generation using CM-H_2DCFDA-loaded islets after 1 h of incubation in 2.2 mM glucose (*WT*, $n = 15$; *KO*, $n = 12$). *I*, detection of ROS-modified proteins in islets (*left panel*) and pancreas (*right panel*) by anti-4-HNE antibody. *J*, concentration of urinary 8-OHdG, a marker of ROS generation (*WT*, $n = 10$; *KO*, $n = 8$).

Deficiencies in Glucose Homeostasis and Insulin Secretion in SMS1-KO Mice Is Partially Rescued by Anti-oxidant Treatment—Our results led us to hypothesize that increased ROS generation seen in SMS1-KO mice underlies the phenotypes seen in these mice and that treatment with anti-oxidants might rescue these conditions (Fig. 6). To test this idea, we supplied the anti-oxidant *N*-acetyl cysteine (NAC) in animal drinking water and then analyzed

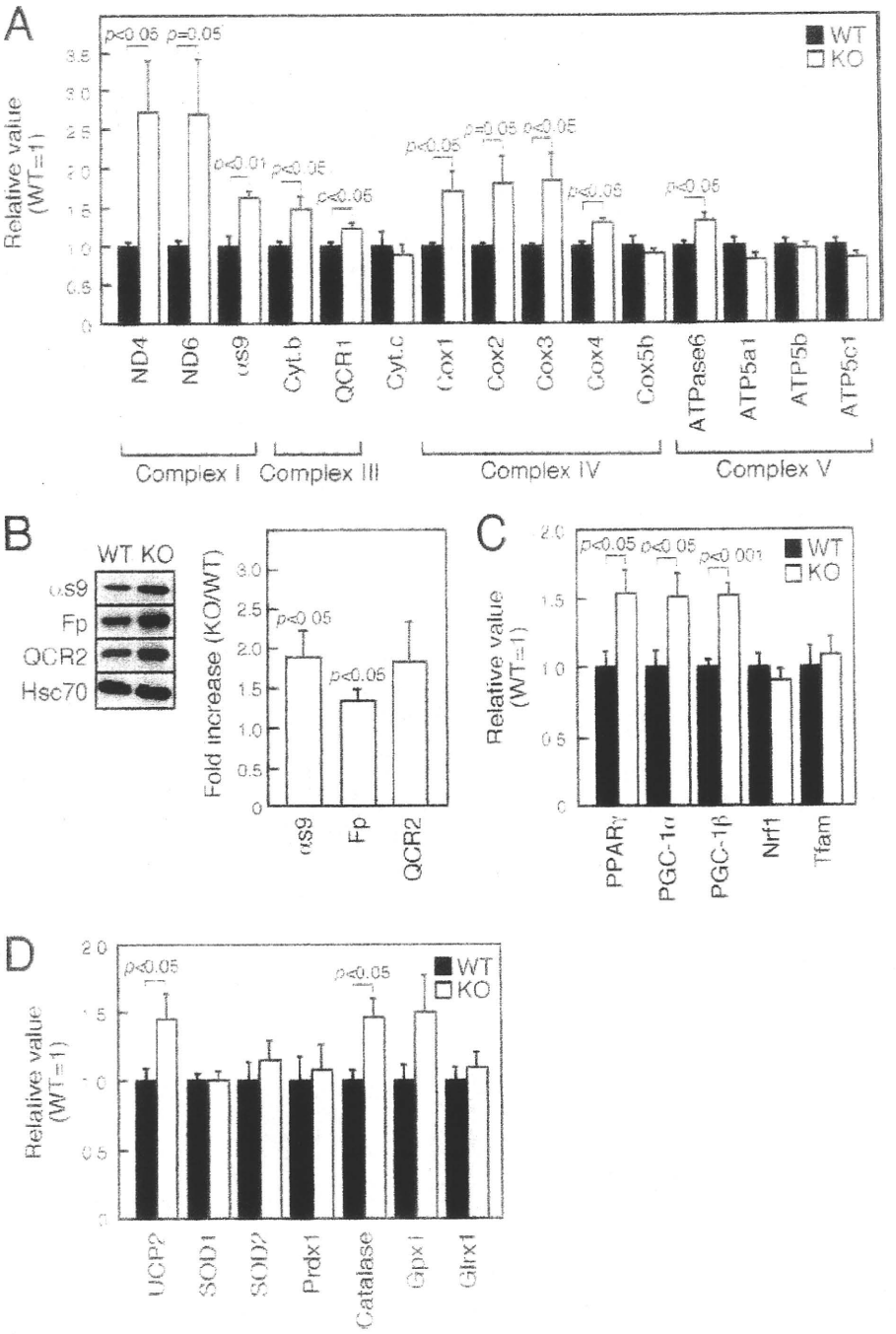

FIGURE 5. **Mitochondrial biogenesis is enhanced in SMS1-KO islets.** mRNA or protein expression in islets isolated from 12–16-week-old mice was examined by quantitative RT-PCR or immunoblot analysis, respectively. *A*, expression levels of genes encoding mitochondrial respiration complex factors were assessed. Islets isolated from two mice of the same genotype served as one sample. Individual measurements were normalized to β-actin expression, and the wild-type group average was set to 1. $n = 6–8$ samples per group. *B*, expression levels of mitochondrial respiration complex proteins were assessed by immunoblot analysis. Islets isolated from four mice of the same genotype constituted one sample. Individual measurements were standardized using Hsc70, and the wild-type group average was set to 1. Increases in ratio in KO *versus* WT are shown as *Fold increase*. $n = 3$ samples per group. *C*, expression levels of genes encoding mitochondrial biogenesis proteins were assessed. $n = 6–12$ samples per group. *D*, expression levels of genes encoding UCP2 and ROS detoxification enzymes were assessed. $n = 8–12$ samples per group.

urinary levels of 8-OHdG, a marker of ROS generation. NAC-treated SMS1-KO mice showed significantly decreased 8-OHdG levels compared with untreated SMS1-KO mice (Fig. 6*A*). Furthermore, NAC treatment improved glucose uptake and insulin secretion in SMS1-KO mice (Fig. 6, *B* and *C*). Surprisingly, NAC-treated SMS1-KO mice showed reduced lethality (Fig. 6*D*). Overall, these results indicate that increased ROS production underlies insulin secretion deficiencies and lethality seen in SMS1-KO mice.